

**ULTRA-WIDEBAND BASED UAV POSITIONING IN GNSS  
DENIED ENVIRONMENT**

KUNWOO PARK

A THESIS SUBMITTED TO  
THE FACULTY OF GRADUATE STUDIES  
IN PARTIAL FULFILLMENT OF THE REQUIREMENTS  
FOR THE DEGREE OF  
MASTER OF SCIENCE

GRADUATE PROGRAM IN EARTH AND SPACE SCIENCE  
YORK UNIVERSITY  
TORONTO, ONTARIO

APRIL 2020

© KUNWOO PARK, 2020

## ABSTRACT

GNSS-IMU-based navigation has been introduced in the mid-90s and still a key component of UAV navigation. However, it has a critical drawback to operate in downtown core areas where high-rise buildings often interfere with signals from GNSS. One emerging solution is to position UAV using Ultra-Wideband (UWB) due to its robustness to multipath and cm-level ranging error. This thesis is a study about GNSS-denied localization based on UWB ranging.

UWB-based positioning requires an understanding of UWB ranging and calibration. For many years, total stations have and continue to be the gold standard for measuring distances using electronic distance measurement (EDM) technology. Consider, current and coming ranging technologies are often compared with total stations. I investigate UWB ranging accuracy by comparing the UWB range with total station measurements in the field test.

Despite the importance of UWB based positioning, there has been no benchmark dataset provided for the evaluation of the related algorithms. I provide UWB-IMU-based UAV positioning dataset in GPS denied environments. I set up our systems in an indoor space and installed four anchors. As ground truth, I tracked the 360-degree mini prism mounted on the UAV using ATR (automatic target recognition) functionality of Leica Nova MS60 MultiStation, an instrument that is combining all available measurement technologies with millimeter-level accuracy at 10Hz. A total of five datasets was acquired with intensive lateral and vertical motions by manually navigating the UAV.

Using the collected data set, I first develop multilateration. Multilateration is an independent position estimation process using range measurement. One of the major problems in multilateration is flip ambiguity, which occurs huge errors. A method for obtaining algebraic solutions and correcting flip ambiguity is presented. Corrected solutions are refined with non-linear

optimization to achieve higher accuracy. Experimental results are presented with the collected data set.

The last chapter present an Ultra-Wideband based (UWB) positioning and fuses the data via an inertial measurement unit (IMU) using an extended Kalman filter (EKF). Experimental results are presented with the collected data set. As a result, a developed technique was able to provide positioning within 10cm.

## ACKNOWLEDGMENTS

This thesis would not be possible without the support of many people. I would like to extend my sincere appreciation to them for their help and support throughout my research.

I would like to extend my sincere gratitude to my supervisor, Dr. Gunho Sohn, who provided me with his excellent guidance and great encouragement throughout my Master's program and undergraduate study. Without his valuable advice, I would never have been able to accomplish my research and this thesis. The research process was sometimes difficult, but thanks to his advice and support, I was able to grow into a better scientist.

I would like to extend my gratitude to Dr. Costas Armenakis, as my supervision committee member, who offered many valuable advices and insightful discussions and suggestions on my research. In addition, I would like to thank Dr. Mozhdeh Shahbazi for her critical suggestions on my research work.

Also, I would like to thank all the colleagues of Sohn's lab. Special thanks are given to Dr. Jungwon Kang for his constant and strong help with the implementation and experiment. I would never have been able to conduct experiments and develop my research without him. Also, thanks for the supports from Dr. Connie Ko, Dr. Pio Claudio, Dr. Yujia Zhang, Ali Baligh, Kivanc Babacan, Maryam Jameela, Zahra Arjmandi, Muhammad Kamran, Afnan Ahmad, Kang Zhao, Sun Park, David Recchia, Phillip Robbins and other members of the lab.

I would like to thank my friends, Kang Zhao, Leihan Chan, Ali Baligh and so on. I wish to appreciate the financial supports from Natural Sciences and Engineering Research Council of Canada (NSERC), Center for geomatics of Quebec (CGQ) and York University.

## TABLE OF CONTENTS

<b>Abstract.....</b>	<b>ii</b>
<b>Acknowledgments .....</b>	<b>iv</b>
<b>Table of Contents .....</b>	<b>v</b>
<b>List of Tables .....</b>	<b>ix</b>
<b>List of Figures.....</b>	<b>x</b>
<b>List of Abbreviations .....</b>	<b>xii</b>
<b>Chapter 1 Introduction.....</b>	<b>1</b>
1.1 Motivation .....	1
1.2 Aims and Research Challenges .....	4
1.3 Contributions.....	6
1.4 Thesis Outline .....	7
<b>Chapter 2 Background .....</b>	<b>9</b>
2.1 Positioning techniques.....	9
2.1.1 Time of Arrival (ToA) .....	9
2.1.2 Time Difference of Arrival (TDoA) .....	10
2.1.3 Angle of Arrival (AoA) .....	11
2.1.4 Received Signal Strength (RSS).....	11
2.2 Various sensors for UAV positioning .....	12
2.2.1 Ultra-wideband .....	12
2.2.2 Image-based .....	13
2.2.3 Dead-reckoning.....	14
2.3 Positioning algorithms.....	14

2.3.1	Multilateration.....	14
2.3.2	EKF.....	15
<b>Chapter 3 Ultra-wideband range calibration.....</b>		<b>16</b>
3.1	Introduction .....	16
3.2	UWB structure (Two-Way Time-of-Flight).....	17
3.3	UWB calibration .....	18
3.4	UWB calibration setup.....	19
3.4.1	Equipment.....	19
3.4.2	Field Calibration procedure .....	20
3.5	Experimental Results.....	22
3.5.1	Residual.....	25
3.5.2	Failure rate .....	25
3.5.3	Standard deviation .....	26
3.6	Summary .....	27
<b>Chapter 4 UWB and IMU Dataset for UAV positioning .....</b>		<b>28</b>
4.1	Introduction .....	28
4.2	Configuration .....	29
4.2.1	UAV platforms and UWB sensors.....	29
4.2.2	Experimental Setup.....	30
4.3	Data Synchronization .....	31
4.4	Data sets .....	33
4.4.1	Set 1 - low speed constant height motion .....	34
4.4.2	Set 2 – low speed gradual downward motion .....	35
4.4.3	Set 3 – Circular motion.....	36

4.4.4	Set 4 – Linear motion.....	37
4.4.5	Set 5 –Complex motion .....	38
4.5	Summary .....	39
<b>Chapter 5 UWB based positioning with Multilateration .....</b>		<b>40</b>
5.1	Introduction .....	40
5.2	Flip ambiguity in multilateration.....	40
5.3	Methodology .....	42
5.3.1	Step 1 - Computation of an algebraic solution.....	45
5.3.2	Step 2 - Correction of a Solution by Symmetric Reflection through Anchor Plane under Flip Ambiguity.....	46
5.3.3	Step 3 - Refinement of a solution using non-linear optimization .....	48
5.4	Experimental results.....	49
5.4.1	Error Analysis in Algebraic Solution.....	52
5.4.2	Effect of the Proposed Correction under Flip Ambiguity.....	52
5.4.3	Effect of Solution Refinement by Non-linear optimization.....	53
5.5	Summary .....	54
<b>Chapter 6 EKF based UAV Positioning Algorithm.....</b>		<b>55</b>
6.1	Introduction .....	55
6.2	Kalman Filter.....	55
6.2.1	Process model .....	56
6.2.2	Equations.....	57
6.2.3	Extended Kalman Filter (EKF).....	58
6.3	IMU driven motion model and measurement model .....	61
6.4	Experimental Results using EKF Methods .....	63

6.4.1	Overview of the positioning results .....	63
6.5	Discussions.....	70
6.5.1	Influence of height on accuracy .....	70
6.5.2	Influence of velocity on accuracy .....	71
6.6	Summary .....	72
<b>Chapter 7 Conclusions and Future works .....</b>		<b>73</b>
7.1	Conclusions .....	73
7.2	Directions for Future Research .....	74
<b>Bibliography .....</b>		<b>77</b>

**LIST OF TABLES**

<b>Table 1.1 Characteristics of metric inspection .....</b>	<b>1</b>
<b>Table 3.1 UWB calibration result.....</b>	<b>23</b>
<b>Table 3.2 UWB calibration parameters .....</b>	<b>23</b>
<b>Table 4.1 Time difference.....</b>	<b>32</b>
<b>Table 4.2 Indoor Q-Drone UAV trajectory datasets. ....</b>	<b>33</b>
<b>Table 5.4 Multilateration results for each step .....</b>	<b>49</b>
<b>Table 6.1 EKF and multilateration results .....</b>	<b>63</b>

## LIST OF FIGURES

<b>Figure 2.1 UWB versus other radio communication systems .....</b>	<b>12</b>
<b>Figure 3.2 Field Calibration (a) set up, (b) antenna center and (c) prism.....</b>	<b>21</b>
<b>Figure 3.3 Linear fit for UWB range calibration.....</b>	<b>24</b>
<b>Figure 3.4 Residual .....</b>	<b>25</b>
<b>Figure 3.5 Failure rate.....</b>	<b>26</b>
<b>Figure 3.6 Standard deviation .....</b>	<b>27</b>
<b>Figure 4.1 UAV platform and sensors.....</b>	<b>30</b>
<b>Figure 4.3. Time Synchronization (a) before synchronized, (b) after synchronized ...</b>	<b>33</b>
<b>Figure 4.4 Set 1.....</b>	<b>34</b>
<b>Figure 4.5 Set 2.....</b>	<b>35</b>
<b>Figure 4.6 Set 3.....</b>	<b>36</b>
<b>Figure 4.7 Set 4.....</b>	<b>37</b>
<b>Figure 4.8 Set 5.....</b>	<b>38</b>
<b>Figure 5.3 Description of UWB tag, UWB anchors and anchor frame. ....</b>	<b>43</b>
<b>Figure 5.4 The proposed algorithm for multilateration, where it consists of major three steps producing initial estimated position, corrected position, and refined position, respectively. ....</b>	<b>44</b>
<b>Figure 5.6 Ground-truth trajectory and estimated position (left column) and absolute error (right column) over time. Green: Ground truth, red: step 1, blue: step 2, cyan: step 3.....</b>	<b>51</b>
<b>Figure 5.7 Step 1 Average MAE of 5 data sets .....</b>	<b>52</b>
<b>Figure 5.8 Step 2 Average MAE of 5 data sets .....</b>	<b>53</b>
<b>Figure 5.9 Step 3 Average MAE of 5 data sets .....</b>	<b>53</b>

<b>Figure 6.1 A complete picture of the operation of the extended Kalman filter .....</b>	<b>60</b>
<b>Figure 6.2 Set 1 - ground-truth trajectory(Black) and estimated position(Red) in 3D space. ....</b>	<b>64</b>
<b>Figure 6.3 Set 2 - ground-truth trajectory(Black) and estimated position(Red) in 3D space. ....</b>	<b>65</b>
<b>Figure 6.4 Set 3 - ground-truth trajectory(Black) and estimated position(Red) in 3D space. ....</b>	<b>66</b>
<b>Figure 6.5 Set 4 - ground-truth trajectory(Black) and estimated position(Red) in 3D space. ....</b>	<b>67</b>
<b>Figure 6.6 Set 5 - ground-truth trajectory(Black) and estimated position(Red) in 3D space. ....</b>	<b>68</b>
<b>Figure 6.7 Ground-truth trajectory and estimated position (left column) and absolute error (right column) over time.....</b>	<b>70</b>
<b>Figure 6.8 (a) Influence of height on z error and (b) VDOP at the center point.....</b>	<b>71</b>
<b>Figure 6.9 Influence of velocity on accuracy: (a) x error vs x velocity, (b) y error vs y velocity and (c) z error vs z velocity. ....</b>	<b>72</b>

**LIST OF ABBREVIATIONS**

AoA	Angle of Arrival
DR	Dead Reckoning
EDM	Electronic Distance Measurement
EKF	Extended Kalman Filter
GNSS	Global Navigation Satellite System
IMU	Inertial Measurement Unit
INS	Inertial Navigation System
NLOS	Non Line of Sight
PS	Photogrammetry System
Q-Drone	Quality-Driven Autonomous Navigation Module
RF	Radio Frequency
RSS	Received Signal Strength
RTK	Real-Time Kinematic
TDoA	Time Difference of Arrival
ToA	Time of Arrival
TW-ToF	Two-Way Time of Flight
UAV	Unmanned Aerial Vehicle
UWB	Ultra-Wideband
VTOL	Vertical Takeoff and Landing

# Chapter 1

## Introduction

### 1.1 Motivation

Infrastructure such as telecom towers, building facades, hydroelectric towers, mine cliffs, and dams have vertical structures that need to be maintained in health status. Managing these structures requires regular inspection, which is made up of two components: metric and visual inspection. Visual inspection refers to physically examining the condition of the infrastructure while metric examination dwells on accurately identifying and measuring facts that may have an impact on the health conditions of the assets. Table 1.1 provides few examples of metric inspections required for different vertical structures that are subjects of study in inspection project.

Table 1.1 Characteristics of metric inspection

Structure	Facts/signs to be measured	Concerns	Required information
Building Facade	Infiltrations, rust or efflorescence of salt	Cracking, breaking or chipping of masonry or concrete surface	Location, measurement, description and photographs of the defects and as-built drawings of the construction work of the façades
	Thermal anomalies	Energy deficiency	
	Cracking at corners of window openings	Corrosion of concealed steel support mechanisms	
Telecom Tower	Changes in length, location and orientation of antennas	Effects on polarization and direction of signal emission	Drawings of tower profile, cross sections, site layout, single sections and parts as well as guy-wires lengths and directions
	Changes in tower alignment, twist in the structure and beam deflections, rotations of the foundation	Structural failure	
Embankment and Concrete Dams	Cracking, displacement of structural cracks	Slope slide development and foundation problems	As-constructed drawings, maps, plans, photos as well as measurements and descriptions of defects.
	Surface erosion	Changing slopes as well as width and height of embankment or crest	

Current methods of metric infrastructure inspection are prone to error, tedious, costly, and hazardous. For instance, control of metric towers is done by certified climbers by taking photos and measurements with handheld devices. This method is dangerous and errors prone due to the restricted movement of the climbers (Sa & Corke, 2014 b). The use of climbing robots can reduce the risk of inspection but it is not a long-term solution due to the fact that the robots should be in direct contact with the surface to obtain data (Balaguer, Gimenez, & Jardón, 2005; Haynes et al., 2009; Kim et al., 2008). Also, climbing robots require complicated mechanical design and dynamic analysis (Sa & Corke, 2014a).

Static sensor networks are another approach to structural health monitoring or non-destructive evaluation (Bhuiyan, Wang, Cao, & Wu, 2013; Chae, Yoo, Kim, & Cho, 2012). However, this method is faced with many drawbacks. The installation and maintenance costs of static networks make them expensive and cumbersome. This method does not apply to the large volume of urban structures. The sensor network is ineffective because most infrastructure does not require continuous inspection; they only need routine control over a specific period. These drawbacks from various approaches call for innovative technologies for review of vertical structures safely, automatically and remotely.

Significant advances in small vertical takeoff and landing (VTOL) and unmanned aerial vehicles (UAVs) have provided adequate payload, endurance, and operational facility for inspection missions. Low weight UAVs reduce hazards due to their deployment (Sa & Corke, 2014b). Reality capturing technologies such as photogrammetry and laser scanning are integrated with UAVs to improve inspection by collecting three-dimensional data that digitalizes spatial details of infrastructure (Golparvar-Fard, Bohn, Teizer, Savarese, & Peña-

Mora, 2011). Photogrammetry is preferred over laser scanning due to the fact it produces visually interpretable data and a high level of accuracy through the low weight, well-calibrated camera (up to  $\mu\text{m}$ ). Therefore, researchers focus on developing a UAV-photogrammetry system (UAV-PS) as a long-term solution for metric inspection of vertical structures. However, significant gaps and shortcomings in the current research should be addressed.

- **General Challenges of UAV-PSs:** UAV-PSs face challenges in terms of efficient data acquisition and data processing. Surveying grade UAV-PS have critical differences with a conventional aerial photogrammetry system, although it is supposed to yield mm-level accuracy. The differences arise from camera specifications, the performance of navigation sensors and characteristics of unmanned aerial images (Shahbazi, Sohn, Théau, & Menard, 2015).
- **Performance of navigation system:** UAV positioning accuracy via global navigation satellite system (GNSS) based inertial navigation systems (INS) is quite low (2-5 meters), which increases the risks of navigation at the proximity of structures. Tall objects such as buildings can cause GNSS signal blockage and significant multipath errors. This risk also extends to real-time-kinematic (RTK) navigation systems due to signal blockage or base-rover communication-loss. This risk leads to significant degradation of positioning accuracy. Moreover, the exact environment and extension of the vertical structures are usually unknown before the flight. Hence, the flight trajectory, which is conventionally designed from existing Google maps, would not be sufficiently reliable. For this reason, a significant pilot

effort is needed to keeping camera orientation over the features of interest and on the safety of the vehicle because of unknown obstacles (Bruggemann & Ford, 2013; Eschmann, Kuo, Kuo, & Boller, 2013). Thus, it is important to improve the efficiency of flight by developing better path-planning strategies and navigation techniques.

One emerging solution to overcome these limitations is to use ultra-wideband (UWB) sensors (Alarifi et al., 2016) due to its robustness to multipath and NLOS effects. UWB modules can sequentially measure the distance between the tag and each anchor, where the distance can range up to 1000 m and it can be obtained at up to 125 Hz rate with a centimeter-level accuracy (Ruiz & Granja, 2017). Due to these characteristics, UWB sensors have gained popularity for supporting navigation in GNSS-denied environments (Kanellakis, Fresk, Mansouri, Kominiak, & Nikolakopoulos, 2019; Perez-Grau, Caballero, Merino, & Viguria, 2017; C. Wang, Zhang, Nguyen, & Xie, 2017).

## **1.2 Aims and Research Challenges**

As discussed in the previous section, it is obvious that UAV positioning in GNSS-denied environment is essential for UAV-PS for inspection applications. By focusing on UWB ranging sensors and the integration of IMU measurements, this thesis aims to introduce novel UAV positioning systems. To achieve these goals, a number of challenges related to UWB ranging, dataset and algorithm need to be addressed:

- UWB ranging accuracy must be ensured to achieve accurate positioning. Thus UWB ranging has to be well calibrated to remove any bias which can cause huge error in positioning results. There have been several researches on calibration based on time of arrival (Y. Wang, Leus, & Deliç, 2009) but time of arrival method requires time synchronization which make UWB ranging difficult to use. Some calibration research based on received signal strength (Gigl, Janssen, Dizdarevic, Witrisal, & Irahhtauten, 2007) is not suitable for accurate positioning due to its low ranging accuracy. Two-way time of flight ranging method is the most suitable ranging method for positioning due to its high accuracy and asynchronous characteristics. Guo et al. (2016) conducted calibration for TW-TOF in various situation but it was limited to small scale to apply to vertical structure inspection applications.
- UWB based UAV positioning data generation: Despite the importance of UWB and IMU fusion for UAV positioning, there hasn't been much benchmark dataset provided for evaluation of the related algorithms. Raza et al. (2019) provided a dataset for indoor positioning with Bluetooth and UWB systems and motion capture sensors (Raza et al., 2019). However, this dataset only contains 2D ground data so it can be limitedly applied for positioning of UAV. Barral et al. (2019) created a simulator and dataset acquired using UWB (Barral, Suárez-Casal, Escudero, & García-Naya, 2019). This dataset is also limited to 2D ground data. Thus, new dataset for UAV positioning using UWB is necessary for development of algorithms.
- Development of UWB based positioning algorithm using multilateration: Multilateration is an algorithm that is useful in initialization or hovering situations,

but multilateration algorithms often suffer from flip-ambiguity which makes big errors. To apply multilateration effectively, the flip-ambiguity problem must be addressed first. There are several approaches for detecting flip ambiguity in 3D multilateration (W. Liu, Dong, & Song, 2016; Mautz, Ochieng, Brodin, & Kemp, 2007), but none proposes a method for correcting a potentially flipped solution.

- Development of UWB based positioning algorithm using EKF: Measurements from various sensors can be integrated and make accurate prediction through filtering methods. EKF allows using filtering method to a non-linear motion model and a non-linear measurement model. To achieve EKF positioning, an accurate motion model and a measurement model must be employed to the system.

### 1.3 Contributions

The main contribution of this thesis is the development of UWB based UAV positioning system. The specific contribution of this thesis can be summarized as follows:

- Developing an accurate UWB calibration methodology and result: Inspired by Guo et al. (2016), UWB can be calibrated in the ground for better representation for distance. I collect data on a large scale up to 110m, which related to actual positioning distance for infrastructure inspection.
- Developing a UWB based UAV positioning benchmark dataset with ground truth data: IMU data were also collected for better estimation of UAV position. It is expected that researchers are able to use data for testing the positioning algorithm.

- Developing a multilateration algorithm with flip ambiguity correction: First, inspired by Norrdine (2012), I perform multilateration which occurs flip ambiguity. I develop a novel algorithm to correct flip ambiguities that can cause large errors in the multilateration process.
- Developing an EKF based positioning algorithm: I develop an IMU driven model which allow us accurate positioning by fusing UWB and IMU.
- Validation of algorithms: All algorithms will be validated by using the collected data set.

## 1.4 Thesis Outline

This thesis is organized into seven chapters. An overview of the chapters follows:

*Chapter 1* presents an introduction to the motivation of this thesis and the proposed methods and strategy for solving research questions.

*Chapter 2* detail the background information that aids in the understanding of this thesis, and comprehensive literature reviews concerning UWB ranging, multilateration, EKF based positioning.

*Chapter 3* introduces the UWB ranging technology. The two-way time of flight (TW-ToF) ranging technique shall be introduced in detail. Moreover, UWB calibration will be discussed with experimental data.

*Chapter 4* presents data sets I collected for the GNSS-denied environment. I shall describe our experimental setup, configuration, hardware, and software system.

*Chapter 5* presents a UWB based positioning system in the GNSS-denied environment using multilateration.

*Chapter 6* presents a UWB based positioning system in the GNSS-denied environment using Extended Kalman Filter.

*Chapter 7* provides the conclusion of this study and recommendations for future works.

## **Chapter 2**

### **Background**

In this chapter, I review a number of previous research works related to distance estimation, UAV positioning techniques, and algorithms. The first part of this chapter discusses various distance estimation methods. The second part reviews existing UAV positioning techniques. The last part introduces various algorithms for solving the positioning problems.

#### **2.1 Positioning techniques**

In this section, different types of distance measuring methods for multiple systems are described. The distances calculated are used in trilateration between three or more reference points for being able to find the coordinate of the tracked system related to the reference points positions (H. Liu, Darabi, Banerjee, & Liu, 2007).

##### **2.1.1 Time of Arrival (ToA)**

Time of Arrival (ToA) is the simplest of the time-based distance estimation methods but challenging to implement in practice. It is the simplest because it uses one-way communications for the estimations, where units are either dedicated transmitters or receivers, which significantly lowers their complexity. A ranging operation consists of only one transmission, where the transmitter sends a time-stamp of the current time to the receiver.

The data is then compared to the time at the receiving instant, and since the speed of light is a known constant, the distance between the transmitter and receiver can be determined (H. Liu et al., 2007; Long, Shen, Feng, Zhu, & Wang, 2016). It is challenging to implement because the accuracy of the result from ToA depends on the accuracy of the clock synchronization and arrival time measurement (Long et al., 2016; Shi & Ming, 2016; Tiemann, Eckermann, & Wietfeld, 2016a). For instance, a clock error of 1 ns results in an error of roughly 30 centimeters, making it challenging to implement in practice.

### **2.1.2 Time Difference of Arrival (TDoA)**

Time Difference of Arrival (TDoA) uses the difference in arrival time from several known points to calculate the relative distances to each message (H. Liu et al., 2007; Long et al., 2016; Tiemann et al., 2016a). TDoA requires a synchronization between the reference points to ensure that the measuring signal is sent at the same time but, unlike with ToA, the receiver does not need to share this synchronization since the relative difference in arrival time is measured instead of the absolute (Shi & Ming, 2016; Tiemann, Eckermann, & Wietfeld, 2016b). Therefore, the reference point can be connected through a wire which eliminates the need for more complex wireless clock synchronization algorithms. However, the reliability of this method is questionable because if the master point responsible for the synchronization fails to work, the entire system degrades.

### **2.1.3 Angle of Arrival (AoA)**

The angle of Arrival (AoA) uses the angles of two incoming signals to the receiver to determine its position relative to the two fixed reference points (H. Liu et al., 2007; Shi & Ming, 2016). A positioning requires one less fixed point compared to using time-based methods. This significantly reduces the required system hardware, which reduces sources of errors. However, determining the angle of an incoming signal with the required precision is more complicated than time-stamping. This drawback and the reflected signals will adversely impact accuracy. This method is rarely used in NLoS situations than time-based methods (Bogdani, Vouyioukas, Nomikos, Skoutas, & Skianis, 2015; H. Liu et al., 2007).

### **2.1.4 Received Signal Strength (RSS)**

Received Signal Strength (RSS) uses reference points or searched objects as transmitters and the other side as receivers, which facilitates obtaining of the signal strength in decibel in the receivers which was transmitted from the transmitters (Contreras, Castro, & de la Torre, 2017; Neburka et al., 2016; Viswanathan & Srinivasan, 2015). Wi-Fi and Bluetooth are representative RSS-based positioning sensors. RSS is easy to use because it relies on simple measurements of the signal strength. However, the problem is if the reference points and searched object is NLoS of each other since the signal can get absorbed by numerous different types of materials. Therefore, it is suitable for low-cost applications with lower demand inaccuracy (H. Li, 2014; H. Liu et al., 2007).

## 2.2 Various sensors for UAV positioning

This section gives an overview of related works with multiple methods for solving the problem of UAV positioning and technologies. These methods consist of various advantages and disadvantages.

### 2.2.1 Ultra-wideband

In recent years, Ultra-wideband (UWB), which is a promising and accurate ranging technology for positioning, is used by researchers (Mao, Lin, Yu, & Shen, 2018). UWB has tremendous potential for both indoor and outdoor positioning (McLoughlin, Cullen, Shaw, & Bezombes, 2018). Note that UWB ranging sensors first became available in 1990 (Gezici et al., 2005). UWB is a high-speed technology for data communication over the personal area network. This technology is based on transmitting short pulses spread over a wide frequency band with a low power density (Nekoogar, 2005).

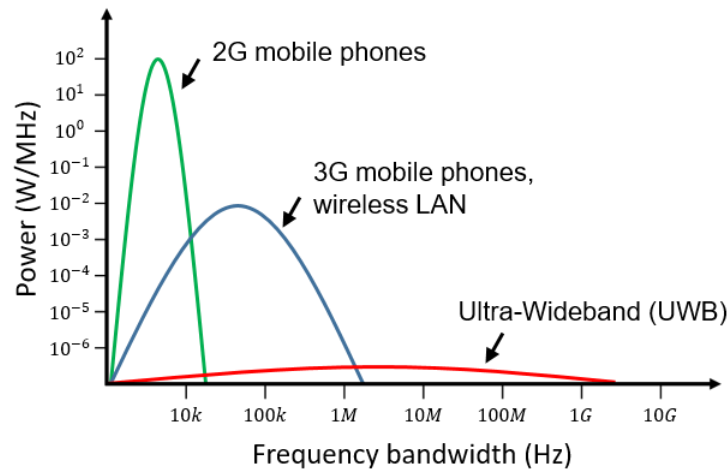


Figure 2.1 UWB versus other radio communication systems

Figure 2.1 shows the difference in the frequency spectrum and power density occupied by different communication standards such as 2G, 3G, and UWB (Vinayak, 2010). The wide bandwidth of UWB allows high accuracy ranging by compressing the edge used for determining the receive time so that accurate time-stamping of a pulse is available without exceeding the energy density limits. It also allows for a high data throughput for communication purposes, and the low-frequency pulses enable the signal to pass through non-metallic obstructions. The ability to pass through obstacles makes UWB technology applicable for NLoS situations like indoor positioning, while total stations require a direct line of sight to measure the distance (Nekoogar, 2005). For these reasons, UWB based positioning gained attention for researchers.

### **2.2.2 Image-based**

Image-based positioning uses a camera to identify objects or people and then localize the position to a coordinate in the horizontal plane. This technique is easy to set up and can use existing cameras, and does not require the target to carry any kind of tracking device. Some form of image processing is needed to find the target in the frame and determine its location. However, more complex environments requiring more sophisticated processing algorithms (Gaspar & Oliveira, 2011). There is also a significant challenge in the cost because a camera with a larger field of view needs to have a higher pixel density to allow for accurate detection of tracking targets. The major disadvantage of this system is the need for a clear LoS to the target, and it can also be affected by the ambient light. The system requires multiple cameras to be installed to cover one area, which makes it expensive and complicated compared to

other systems. It is also undesirable for public applications because it is unethical behavior to record and track people.

### **2.2.3 Dead-reckoning**

Dead-reckoning (DR) uses the last known positioning of the target combined with data from its movement to estimate the new position following a short delay. An accelerometer is used to measure the speed of the moving object (Ksentini, Elhadi, & Lasla, 2014), while a gyroscope gives the angular velocity to determine the direction of the movement. These two units are known as the Inertial measurement unit (IMU), with the possibility of adding a magnetometer to correct for the gyroscopes drift (Luna, Meifeng, Xinxi, Yongjian, & Mingliang, 2015; Perttula et al., 2014). A barometer is used to measure pressure if a position in three dimensions is needed. DR systems are prone to error propagation because every new position is based on the old one. This concept introduces the need for frequent calibration for reliability (Qigao, Biwen, & Yaheng, 2015). Since the DR system is unreliable alone, it is used to improve the accuracy of other technologies.

## **2.3 Positioning algorithms**

### **2.3.1 Multilateration**

Multilateration is a localization method based on measured distances between a tag and a number of anchor points with known locations. For 2-D positioning, distance observations

from two anchors can narrow the solution with two positions; additional information narrows the possibility to a unique location. For 3-D positioning, distance observations from three anchors can narrow the solution with two positions, and more than four observations can provide a unique solution. There are multiple algorithms that solve the 3-D Cartesian multilateration problem. Detailed algorithms are described in chapter 5.

### **2.3.2 EKF**

The extended Kalman filter (EKF) is a very common variation of Bayesian filter, which is developed by modification of Kalman filter (Bishop & Welch, 2001) so that it can be applied to nonlinear system models. Same as the Kalman filter, it is assumed that the noise has zero-mean Gaussian distribution, and the measurement and process noise are independent. It is a very simple and powerful estimator capable of predicting the future states of the system based on the system model, knowledge of the noise, and last measurements. This filter benefits from the state space format for presenting the value of states and the process noise. The filter process includes two development stages, namely, prediction and correction. In the prediction stage, previous estimates of the states are propagated to the next sample time through the system model. In the correction stage, predicted states of the states are updated through the measurement model. Detailed algorithms are described in chapter 6.

## **Chapter 3**

# **Ultra-wideband range calibration**

### **3.1 Introduction**

As stated in chapter 1, the main research objective of this thesis is introduced to accurate positioning of UAVs using UWB ranging sensors. Note that to achieve an accurate position of an UAV, UWB ranging data has to be accurate and very well calibrated. As mentioned before, UWBs are very accurate and new ranging technology that can achieve cm-level accuracy. Yet, for many years, total stations have and continue to be the standard measuring distances using electronic distance measurement (EDM) technology. Total stations are advanced systems and their capabilities are well beyond calculating distances. These advancements include technologies that have benefited the user segment in terms of efficiency in the field. For example, built-in tracking systems have made it possible for a single person to operate a total station. Currently available advanced total stations differ in distance accuracy of  $2\text{mm} + 2\text{ppm}$  to  $5\text{mm} + 10\text{ppm}$  depending on the model. Consider current and coming ranging technologies are often compared with total stations. Here, I investigate UWB ranging accuracy by comparing the UWB range with total station measurements. In section 3.2, I describe UWB ranging structure which uses Two-way Time-of-flight. In section 3.3, UWB calibration method is described by adopting simple linear regression. In section 3.4, the experimental setup is described including equipment and

detailed procedure. In section 3.5, field data and calibration results are analyzed. I summarize this chapter in section 3.6.

### 3.2 UWB structure (Two-Way Time-of-Flight)

In order to understand how to measure distance using UWB, Two-Way Time-of-Flight (TW-TOF) must be introduced. TW-TOF is an asynchronous ranging scheme where a mobile node periodically broadcast a beacon signal containing its time of departure. Unlike a synchronous ranging scheme, the asynchronous ranging does not require synchronising the time of arrival and departure between two nodes (mobile and anchor nodes). Instead, in the asynchronous ranging scheme, each node measures the TOF of the ranging signal in order to estimate a round trip time by obtaining the delay time and consequently the distance between two nodes. The mobile node repeats the ranging procedure with at least three or four anchors nodes for its location to be determined.

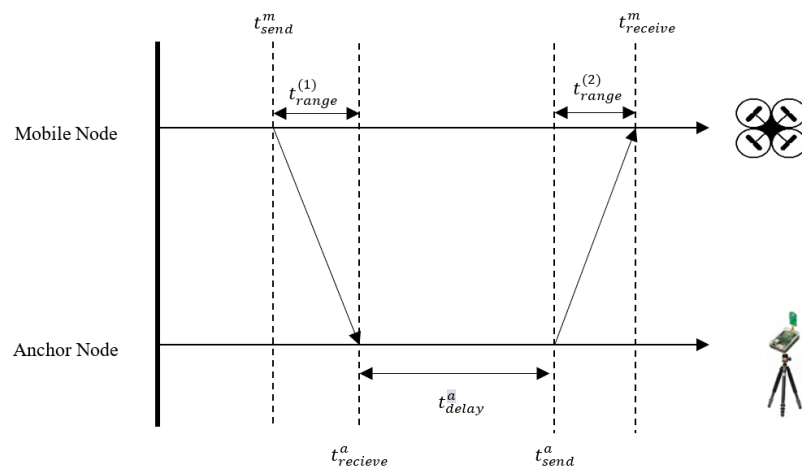


Figure 3.1 TW-TOF asynchronous ranging schema.

As shown in Figure 3.1, UWB mobile nodes mounted in UAV platform transmits a pulsed-RF signal at time  $t_{send}^m$  and receive the request pulse at  $t_{receive}^m$ . A time delay occurred at an anchor node  $t_{delay}^a$  is known, with which a total round trip time  $t_{round}$  and an offset time  $t_{range}$  can be calculated respectively by

$$t_{round} = t_{send}^m + t_{delay}^a + t_{receive}^m \quad (3.1)$$

$$t_{range} = \frac{t_{receive}^m - t_{send}^m - t_{delay}^a}{2} \quad (3.2)$$

Where I assume two offset times measured at the mobile node  $t_{range}^{(1)}$  and  $t_{range}^{(2)}$  in Figure 3.1 are the same. Thus, a relative distance between mobile and anchor node can be calculated by

$$d_a^m = t_{range} * c \quad (3.3)$$

where  $c$  is the speed of light (299,792,458 m/s).

### 3.3 UWB calibration

Inspired by Guo et al. (2016), I discuss a methodology to calibrate the UWB. I can assume linear relationship between UWB range measurement  $r$  and true distance  $d$ . If I consider zero-mean random error  $\epsilon$ , then I can express  $r$  and  $d$  as:

$$r = ad + b + \varepsilon \quad (3.4)$$

Here, the calibration is to find distance  $d$  from the range  $r$ . The classical method is applied for the calibration. According to Montgomery et al. (2012), given  $n$  samples  $(d_i, r_i)$ ,  $i = 1, \dots, n$  collected from different locations, the calibration can be conducted as follows. Linear regression is firstly applied to  $n$  samples to obtain an estimate  $\hat{a}, \hat{b}$ , respectively, for scaling factor  $a$  and bias  $b$  in the measurement model :

$$\hat{a} = \frac{\sum_{i=1}^n (d_i - \bar{d})(r_i - \bar{r})}{\sum_{i=1}^n (d_i - \bar{d})^2} \quad (3.5)$$

$$\hat{b} = \bar{r} - \hat{a}\bar{d} \quad (3.6)$$

where  $\bar{d}$  and  $\bar{r}$  are the mean of  $d_i$ 's and  $r_i$ 's,  $i = 1, \dots, n$ , respectively. After that, the ranging estimate  $\hat{d}$  can be obtained as:

$$\hat{d} = \frac{1}{\hat{a}}\hat{r} - \frac{\hat{b}}{\hat{a}} \quad (3.8)$$

## 3.4 UWB calibration setup

### 3.4.1 Equipment

#### *Ultra-wideband transceiver (TimeDomain PulsON440)*

The PulsON® 440 (P440) module is an Ultra Wideband (UWB) radio transceiver operating between 3.1 and 4.8 GHz made TimeDomain. It uses Two-Way Time-of-Flight (TW-TOF) ranging to

measure the distance between two or more P440s. These measurements have an accuracy of  $<2$  cm and are provided at rates up to 125 Hz. It can be operated up to 500 meter. It operates with very low power transmissions less than  $50\mu\text{W}$ . The energy in each transmitted pulse can be summed to increase the Signal-to-Noise Ratio (SNR) of received transmissions. Each time the number of pulses sent is doubled, the SNR of the received signal will double (increase by 3 dB). This can double the time required to complete the entire transfer. The transmission strength is not increased, rather more energy is summed to improve reception. This applies to all transmissions regardless of whether the transmission is intended for ranging, radar, or communications.

#### ***Total station (Leica Nova MS60 MultiStation)***

MS60 is a MultiStation which is a combination of a Terrestrial Laser Scanner (TLS) and Total Station (TS) made by Leica Geosystems. The MultiStation provides an angular accuracy of 1" (according to ISO 17123-3), and an EDM measurement accuracy is 1 mm + 1.5 ppm onto the prism (according to ISO 17123-4) and 2 mm + 2 ppm onto any surface.

#### ***Prism (Leica GMP101)***

GMP101 is round mini prism made by Leica Geosystems which has Prism constant of +17.5mm, centring accuracy 1.0mm, range 2,000m. It has spike on the back of the prism so I can pin point the UWB antenna that I aim to measure.

### **3.4.2 Field Calibration procedure**

Figure 3.2 (a) shows the field calibration setup. Detailed procedure is described as follows:

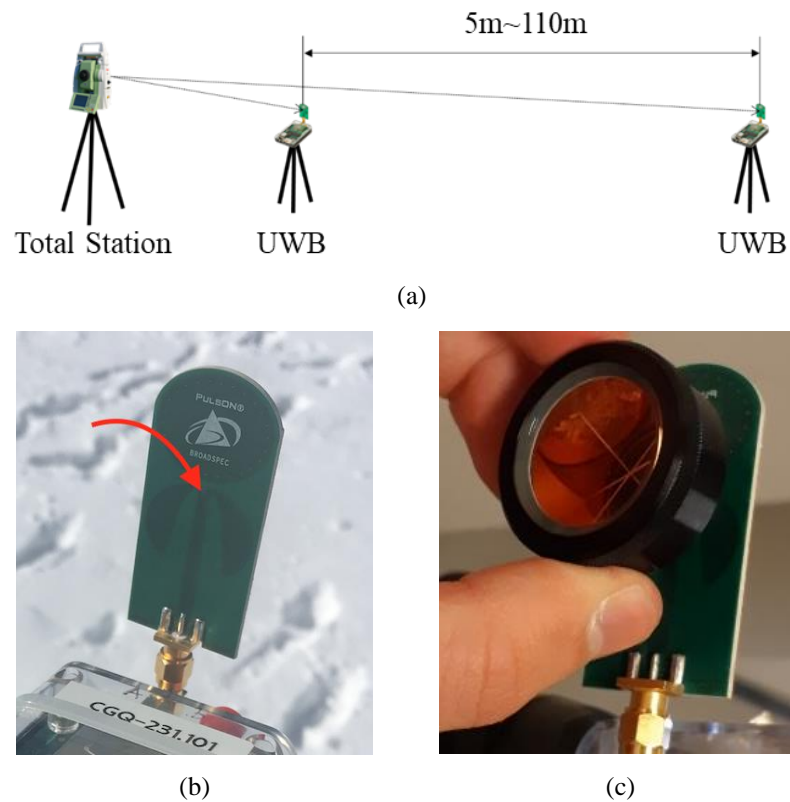


Figure 3.2 Field Calibration (a) set up, (b) antenna center and (c) prism

- A soccer field on York University Keele campus was selected for the experiment that was relatively flat and provided approximately 150 meters of unobstructed space.
- A Nova MS60 Leica total station was leveled in one corner of the field.
- A backsight was established on a light pole that roughly aligned with the experiment setup. A tripod was set up with UWB approximately 5 meters from the total station.
- The orientation of UWB was kept consistent for both stations. The face of the antenna seen in the picture below faced the total station.
- The total station was used to measure a distance of 5 meters between the first tripod with UWB and the second tripod with UWB. This was done by using a reflectorless

mode taking a distance measurement to the person holding the second UWB tripod. Communication signals were used to instruct the person holding the second UWB tripod for both distance and alignment correction.

- To achieve an accurate total station distance, a prism was held over the UWB antenna to reflect the pulse in a similar orientation for each trial. For this measurement, the total station setting was changed to the reflector. The prism was placed over the center of an antenna, as shown in Figure 3.2 (b) and (c).
- A test trial of the UWB was completed at 5 meters to ensure that the system was operating appropriately.
- It was ensured that no obstructions were introduced during the UWB data collection period for all trials.
- After both total station and UWB data collection was completed at a given distance, the second tripod was moved further.
- One thousand measurements were completed from 5m to 45m in 5m increment and from 50m to 110m in 20m increment.

### **3.5 Experimental Results**

Using Excel, the data collected in the experiment is analyzed to extract key statistics, such as averages, standard deviations, calibration parameters. I tried 1000 UWB measurements at each point, and some of the trials fail to measure distance. After removing all failed measurements (which registered as a value of 0) and obvious outliers, statistics were calculated. The results are summarized in Table 3.1. A brief distance between two UWB is

shown in the first column. Next, the average ranges by UWB and total station measurement ground truth are found. After then, residuals are calculated by subtracting total station measurement from average UWB measurement. I also investigate the failure rate and the standard deviation among the thousand UWB measurement at a point.

Table 3.1 UWB calibration result

	UWB (mm)	Total Station (mm)	Residual (mm)	failure rate (%)	StD(mm)
5m	5024.31	5046.88	-22.57	8.10	2.46
10m	9998.18	10019.62	-21.43	7.10	2.20
15m	14963.77	14987.39	-23.62	5.80	3.40
20m	20007.35	20030.77	-23.42	8.00	3.03
25m	24991.89	25012.77	-20.88	6.30	1.93
30m	29952.38	29969.54	-17.16	6.50	12.39
35m	34965.31	34949.02	16.29	7.50	14.80
40m	40049.80	40072.37	-22.57	6.60	1.98
45m	45037.82	45059.26	-21.44	6.70	2.34
50m	49713.55	49716.67	-3.12	0.60	13.04
70m	70666.45	70658.66	7.79	0.70	4.07
90m	90300.22	90297.90	2.32	3.90	3.01
110m	110864.50	110864.60	-0.10	4.10	2.91
Mean			-11.53	5.53	5.20

Table 3.2 UWB calibration parameters

$\hat{a}$	1.0003
$\hat{b}$ (mm)	-23.4237

In Figure 3.3, UWB range measurements were plotted, and a linear fit was drawn between the points. The x-axis represents the EDM range, and the y-axis represents the UWB range. The calibration result is a scale factor  $\hat{a}$  of 1.0003 and a bias  $\hat{b}$  of -23.42 mm as shown in

Table 3.2. Based on this calibration, I can expect -22.02mm of UWB bias at 5m, -9.42mm at 50m, 0.38mm at 85m and 7.38mm at 110m. These results meet the manufacturer's error standard of 2 cm. Detailed analysis is shown in the following sections.

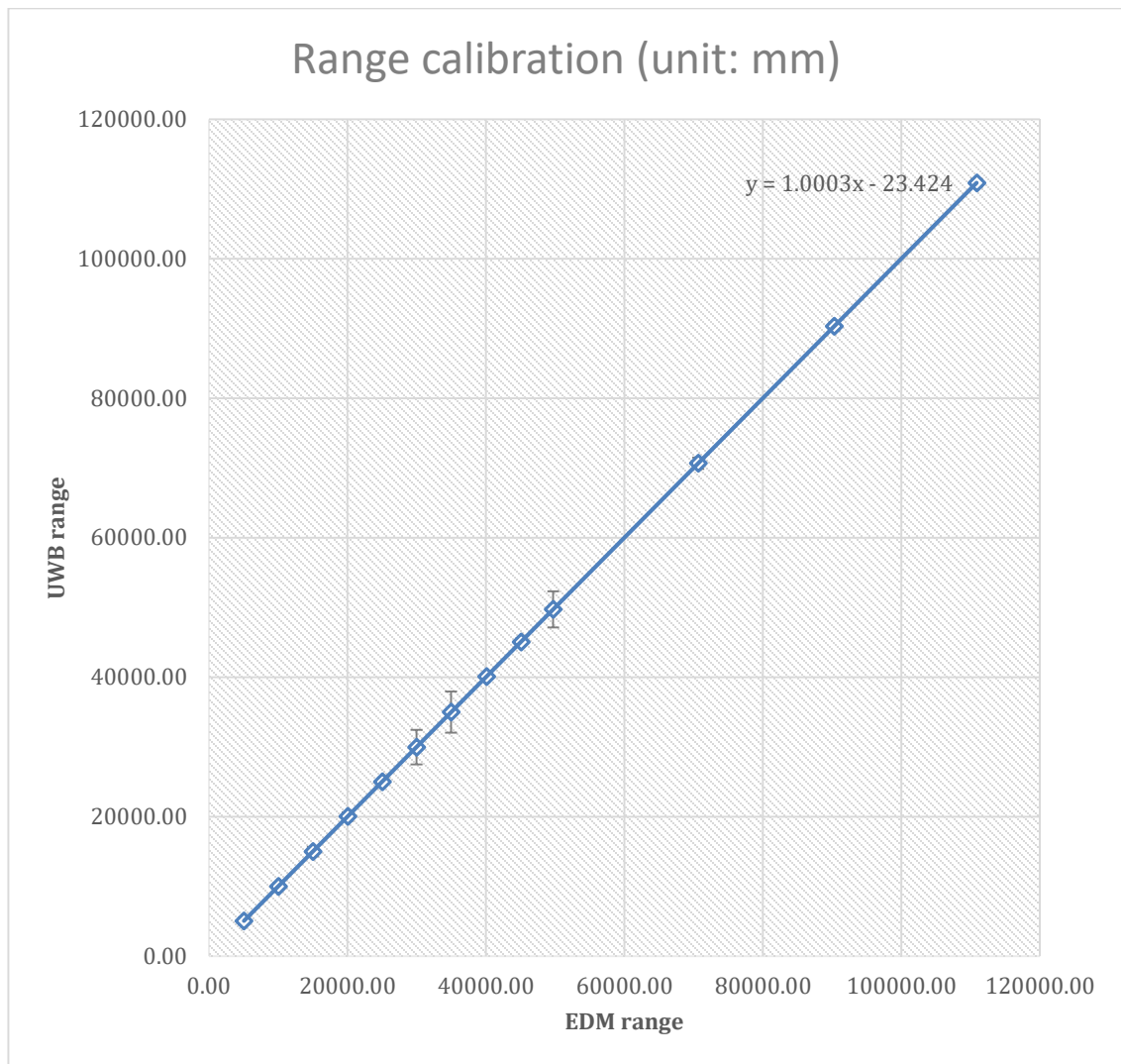


Figure 3.3 Linear fit for UWB range calibration

### 3.5.1 Residual

In Figure 3.4, the UWB range measurement residual is plotted at each distance. The results generated in this experiment showed an average residual of -11.53 mm between UWB and total station measurements. Interestingly, this residual was not shown to grow as a function of distance. The minimum residual appeared in 15m, and the maximum one was at 35m. The absolute residual was smallest at 110m. From 50m to 110 meters, absolute residuals decrease noticeably. This shows that the best operation range is after 50m.

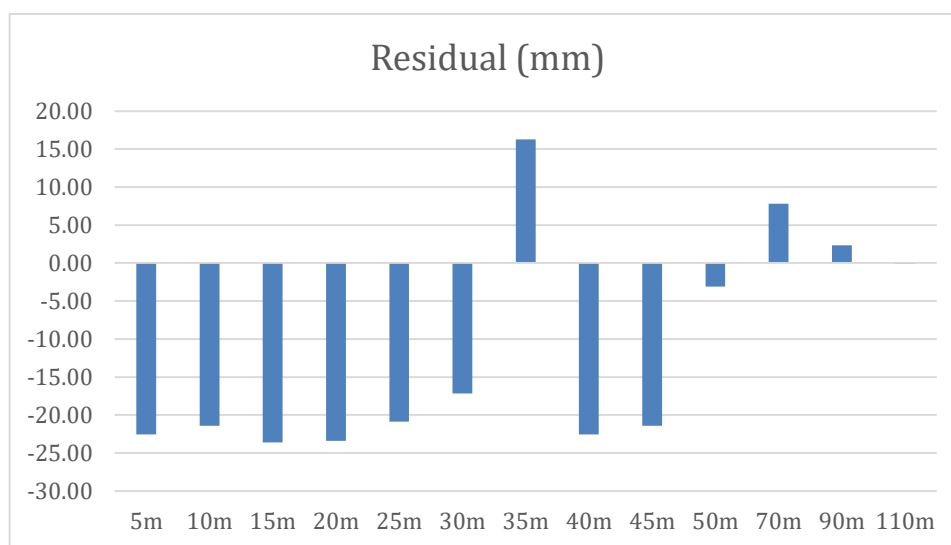


Figure 3.4 Residual

### 3.5.2 Failure rate

Failure to measure the distance can happen due to low power of returned signals. In Figure 3.5, the failure rate is plotted at each distance. The failure rate is important because it can reduce the frequency of measurements. The results generated in this experiment showed an average failure rate of 5.53 %. No significant correlation was found between the failure rate

and the distance within the experimental conditions I performed. The minimum failure appeared in 50m, and the maximum one was at 5m. At 50m and 70m, the failure rate was 0.6% and 0.7%, respectively, and it varies at other distances from about 4% to 8%. This failure happens randomly, so that I have to consider this in our system design. When UWB frequency is 125Hz, the actual frequency can be decreased to 110Hz in the worst case.

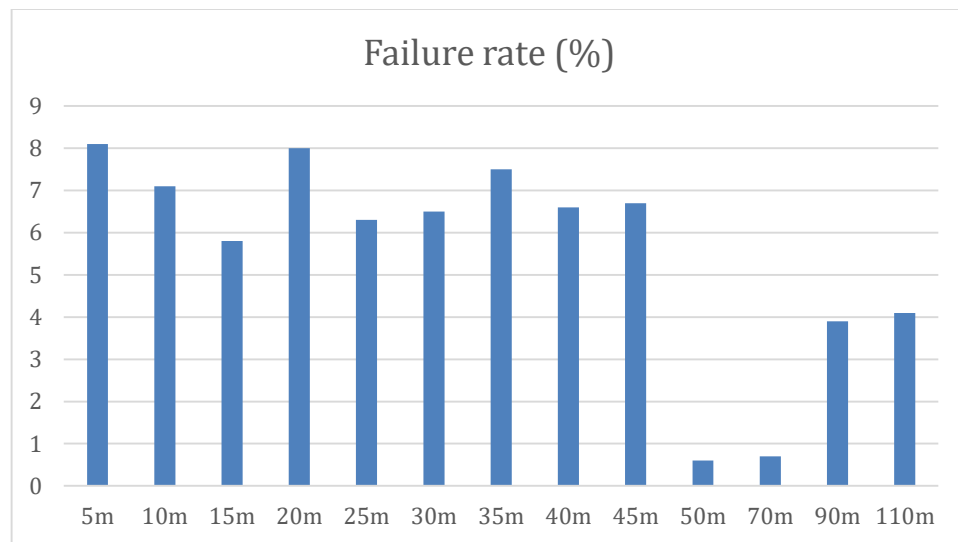


Figure 3.5 Failure rate

### 3.5.3 Standard deviation

In Figure 3.6, the standard deviation rate is plotted at each distance. The results generated in this experiment showed an average standard deviation of 5.20mm. No significant correlation was found between the standard deviation and the distance within the experimental conditions I performed. The minimum standard deviation appeared in 25m as 1.93mm, and the maximum standard deviation was at 35m as 14.80mm. At 30m, 35m, and 50m, the standard deviation was higher than the others. These occurrences did not show a specific

pattern. However, at other places, the standard deviation was 2mm to 4mm. This shows that UWB has very high precision on ranging.

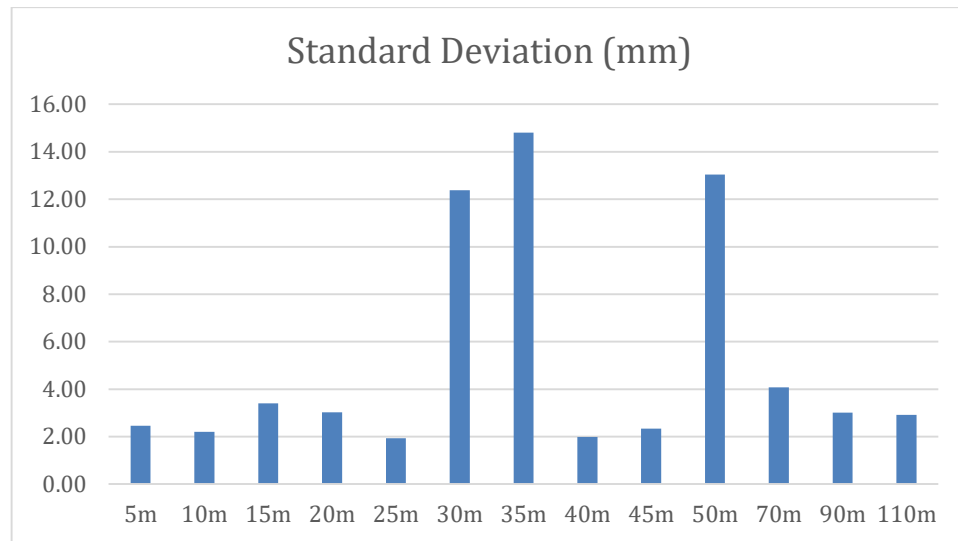


Figure 3.6 Standard deviation

### 3.6 Summary

In this chapter, UWB calibration was conducted to understand UWB ranging and improve accuracy of positioning. As a result, we could find linear relation between UWB range  $r$  and true range  $d$  as  $r = ad + b$  with scale factor  $a$  as 1.00028 and a bias  $b$  as -23.42 mm. This results meet the manufacturers accuracy limit which is less than 2 cm. Average residual is -11.53mm, average failure rate is 5.53% and average standard deviation is 5.20mm. Overall, considering centimeter level accuracy and high frequency with about 5% of failure rate, we can expect accurate positioning of UWB by UWB ranging.

## **Chapter 4**

# **UWB and IMU Dataset for UAV positioning**

### **4.1 Introduction**

In the previous chapter, I explained the need of UWB in the GNSS-denied environment. Due to high frequency up to 125 Hz and cm level accuracy, UWB has a high potential for the GNSS-denied environment. For GNSS based positioning system, various methods are combined with GNSS to improve accuracy (Benini, Mancini, & Longhi, 2013) by fusing with INS (Abdelkrim, Aouf, Tsourdos, & White, 2008; Nemra & Aouf, 2010), Vision (Sohn, Lee, Kim, & Kee, 2008; Tisdale, Ryan, Kim, Tornqvist, & Hedrick, 2008) or hybrid approach of INS and Vision (Rady, Kandil, & Badreddin, 2011). UWB based positioning can be improved with the aforementioned method. In particular, since most UAVs have IMUs, researchers often adopt IMU for improving accuracy. For this reason, a lot of researches for UAV positioning using UWB and IMU fusion has been studied. Recent papers from 2016 used UWB and IMU (Miraglia, Maleki, & Hook, 2017), UWB, IMU and Lidar (K. Li et al., 2016), UWB, IMU and Radar (Zahran et al., 2018), UWB and monocular camera (Tiemann, Ramsey, & Wietfeld, 2018), UWB and RGB-D camera (Perez-Grau et al., 2017).

Despite the importance of UWB and IMU fusion for UAV positioning, there has been no benchmark dataset provided for the evaluation of the related algorithms. In this chapter, I generate data set as a benchmark for UAV positioning in GNSS denied environment. I

collect the UWB range and IMU data for UAV positioning. As ground truth, I adopt robotic total station which can track UAV in high accuracy. I first describe the configuration, including UAV platforms and UWB sensors, and how I set the environment in section 4.2. Secondly, I describe how I synchronize between ground truth data and collected UWB and IMU data in section 4.3. After synchronization, I get five different data sets. The detailed trajectory and characteristics of each data set are explained in section 4.4.

## **4.2 Configuration**

### **4.2.1 UAV platforms and UWB sensors**

Our drone system for the experiment is DJI M100 UAV as shown in Figure 4.1. The accessories including the battery, an Intel NUC and an UWB receiver were mounted on DJI platform on the lowest part of UAV and a 360-degree mini prism under its nose. The total station track the prism and obtains the ground truth position of the UAV during the flight. A PlusON® 440 (P440) UWB module provides us distance measurements at 2 centimeters accuracy over a range of 1000 meters in clear-sighted situations. Five UWB modules including four anchors and one receiver mounted on the UAV work together up to 125 Hz. IMU mounted on UAV provides height, orientation, angular velocity and acceleration data at 100 Hz. The receiver request distance from anchors in round-robin type arrangement. Each anchor sends position data at 10 Hz, thus four anchors the frequency would be 40 Hz. The data are acquired from sensors using Robot Operating System (ROS) kinetic.

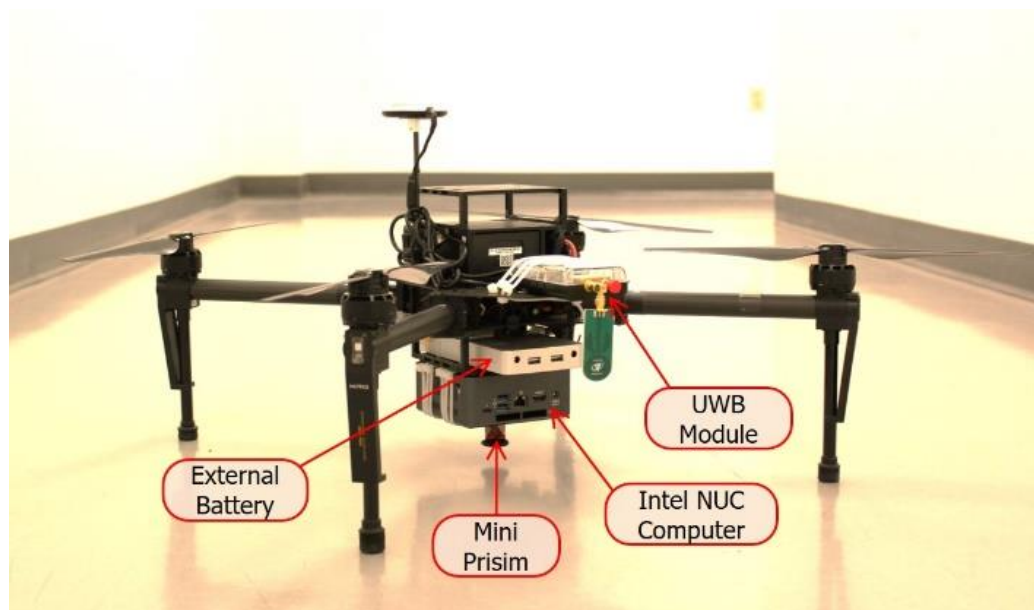
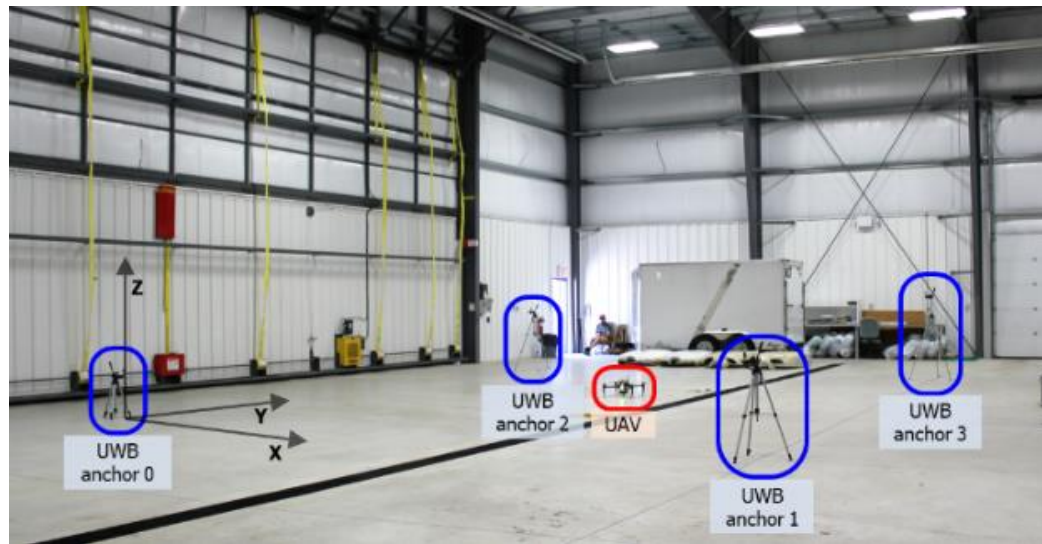


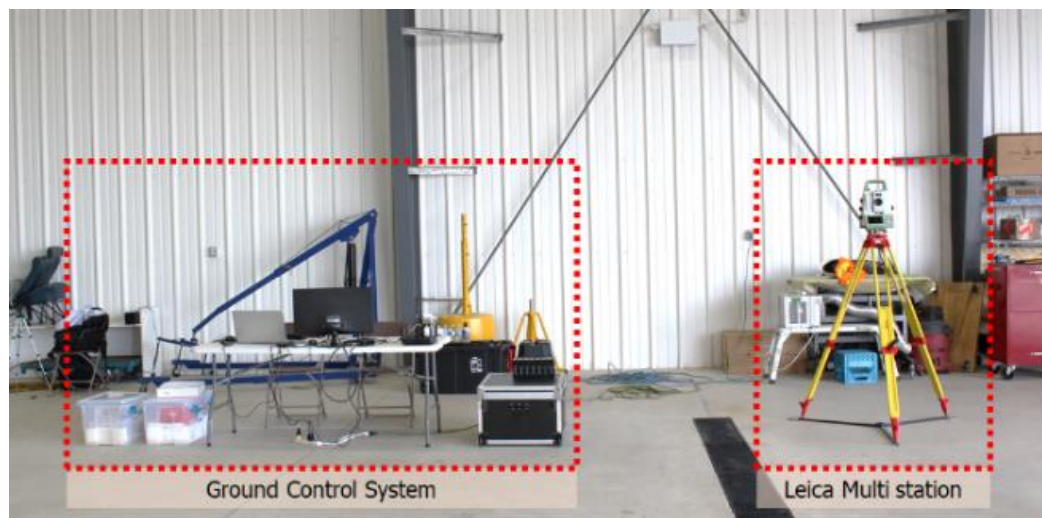
Figure 4.1 UAV platform and sensors

### 4.2.2 Experimental Setup

I set up our systems indoors in a  $26\text{m}\times 33\text{m}\times 10\text{m}$  space (width, length and height respectively) that was a GNSS denied area. Our UWB setup is shown in Figure 4.2 (a). I installed four anchors in these four coordination  $(0.00\text{m}, 0.00\text{m}, 0.62\text{m})$ ,  $(8.51\text{m}, 0.00\text{m}, 0.96\text{m})$ ,  $(-0.26\text{m}, 10.77\text{m}, 1.32\text{m})$ ,  $(8.25\text{m}, 10.84\text{m}, 1.58\text{m})$ . Our ground control system and total station are shown in Figure 4.2 (b). The ground control system and onboard computer on UAV are connected via Wi-Fi to operate the ROS. I tracked the 360-degree mini prism mounted on the UAV using ATR (automatic target recognition) functionality of Leica Nova MS60 MultiStation an instrument which combining all available measurement technologies with millimetre level accuracy at 10Hz. Total five dataset acquired by manually navigating the UAV and covering the specified space.



(a)



(b)

Figure 4.2 Experimental Setup (a) UWB (b) Ground control system

### 4.3 Data Synchronization

To retrieve the ground truth of the UAV position, I tracked UAV with the total station. Since the UAV and total station use different time system, both times of system has to be synchronized. In order to synchronize the time, I used IMU height and total station height.

Notation  $t_{UAV}$  represents the time system used in UAV. Since the ROS system collects UWB and IMU data set, IMU and UWB are synchronized. Notation  $t_{TS}$  represents the time system used in the total station. To synchronize both systems, I have to find time difference  $\alpha$  between two systems.

$$t_{UAV} = t_{TS} + \alpha \quad (4.1)$$

In order to find  $\alpha$  I take the arguments of the minima which minimize square sum of height difference.

$$\alpha = \arg \min_{\alpha} \sum (H_{UAV,t_{UAV}} - H_{TS,t_{TS}+\alpha})^2 \quad (4.2)$$

Here  $H_{UAV,t_{UAV}}$  is height from IMU at  $t_{UAV}$  and  $H_{TS,t_{TS}+\alpha}$  is height from total station at  $t_{TS} + \alpha$ . Calculated  $\alpha$  is shown in Table 4.1.

Table 4.1 Time difference

Dataset	Set 1	Set 2	Set 3	Set 4	Set 5
$\alpha$	35.171s	49.068s	59.453s	35.319s	36.322s

Figure 4.3 shows the graphs of set 1 before(left) and after(right) synchronization. I can visually see the peaks and trends of the graphs are corresponding. However, I can also see the significant discrepancy between IMU height and total station height. This shows drift of IMU can cause large errors if we use it for positioning solely. By fusing with UWB sensors, IMU drift can be corrected properly and achieve accurate positioning.

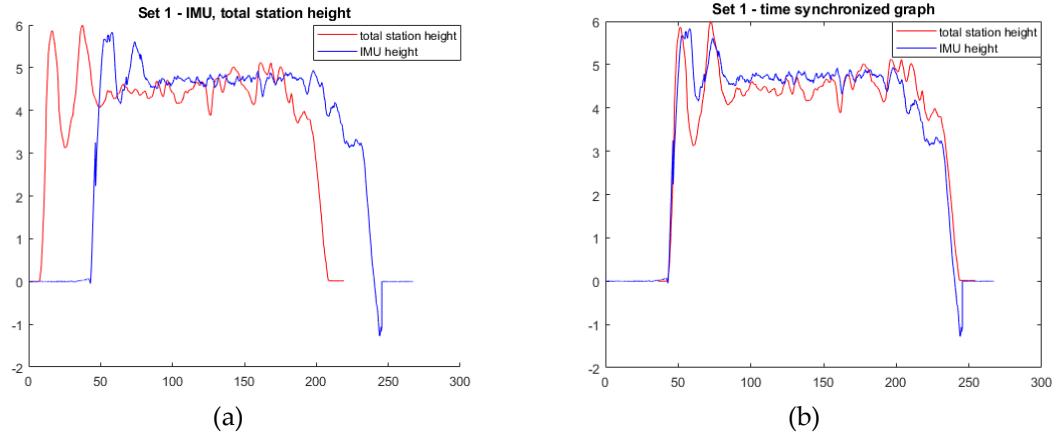


Figure 4.3. Time Synchronization (a) before synchronized, (b) after synchronized

## 4.4 Data sets

Total of five datasets acquired by manually navigating the UAV and covering the specified space with different speed and path. After data synchronization, the benchmark data set was acquired includes IMU, UWB, and ground truth position of UAV in the same time system. The data are briefly stated in Table 4.2. The detailed trajectory is described in the following session.

Table 4.2 Indoor Q-Drone UAV trajectory datasets.

Dataset	Duration	Travelled distance	x-min x-max	y-min y-max	z-max
Set 1	175.733s	138.831m	2.592m 4.745m	1.779m 12.689m	6.910m
Set 2	212.171s	167.494m	-0.281m 8.164m	-1.356m 13.082m	6.087m
Set 3	241.269s	210.485m	-0.474m 7.916m	-0.030m 9.970m	7.164m
Set 4	363.491s	298.466m	-0.440m 8.256m	0.207m 8.474m	6.212m
Set 5	394.531s	448.229m	-1.403m 9.390m	-1.184m 10.174m	5.347m

#### 4.4.1 Set 1 - low speed constant height motion

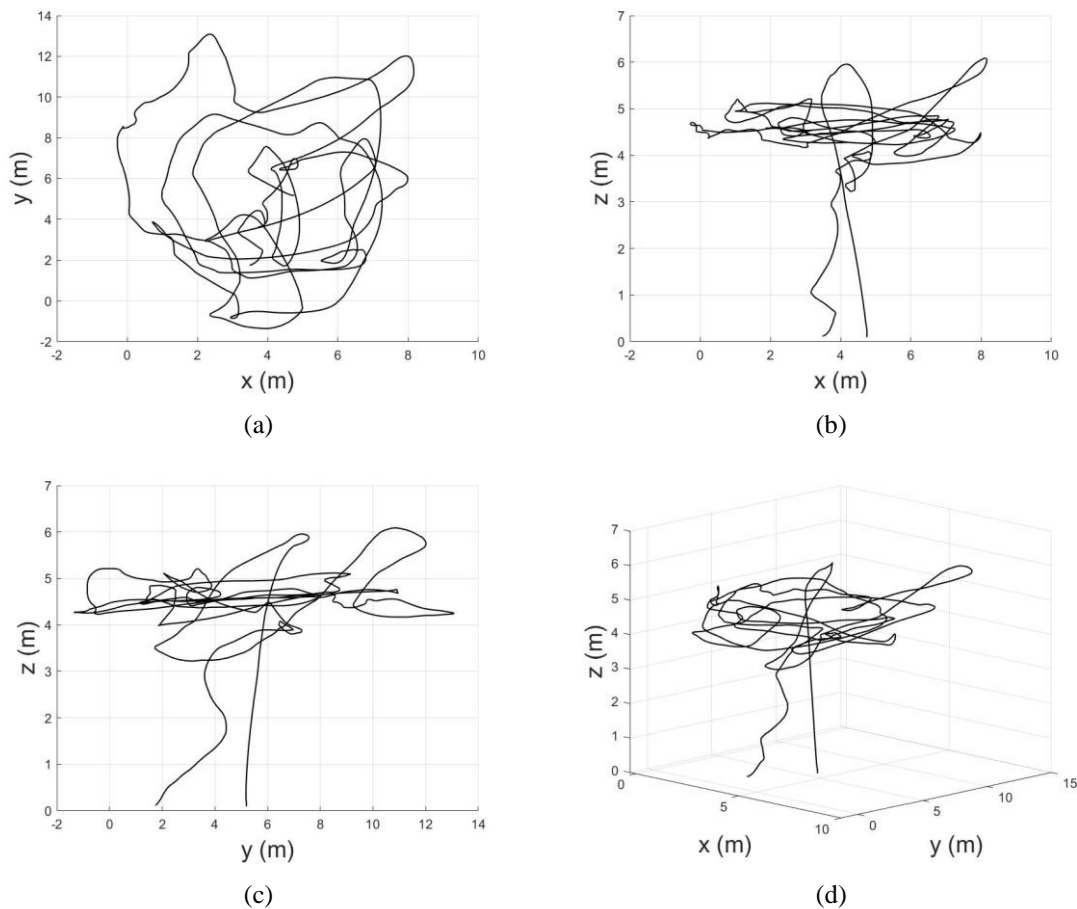


Figure 4.4 Set 1

In this flight, UAV mainly flew in 4.5 meters of height at an average speed of 0.79m/s. A total of 10155 UWB range and 26722 IMU data were measured. Due to the relatively constant height and slow speed of UAV, I can expect higher accuracy than other datasets. This data is used for testing algorithms for a simple trajectory.

#### 4.4.2 Set 2 – low speed gradual downward motion

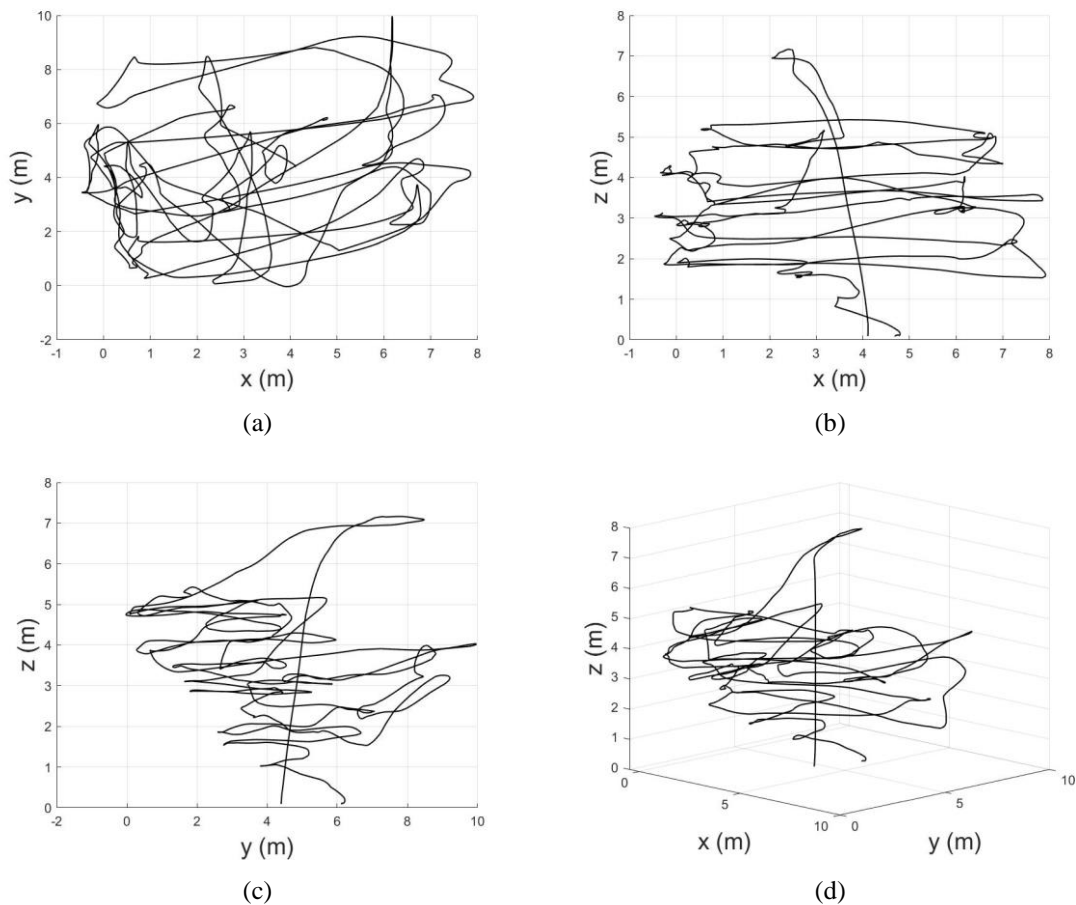


Figure 4.5 Set 2

In this flight, UAV flew randomly at an average speed of 0.79m/s. A total of 11871 UWB range and 30836 IMU data were measured. After taking off of the UAV, it gradually goes down until landing while moving randomly on XY-plane. Due to it has low speed and gradual downward movement, I expect this data can be used for checking the effect of high to the accuracy.

### 4.4.3 Set 3 – Circular motion

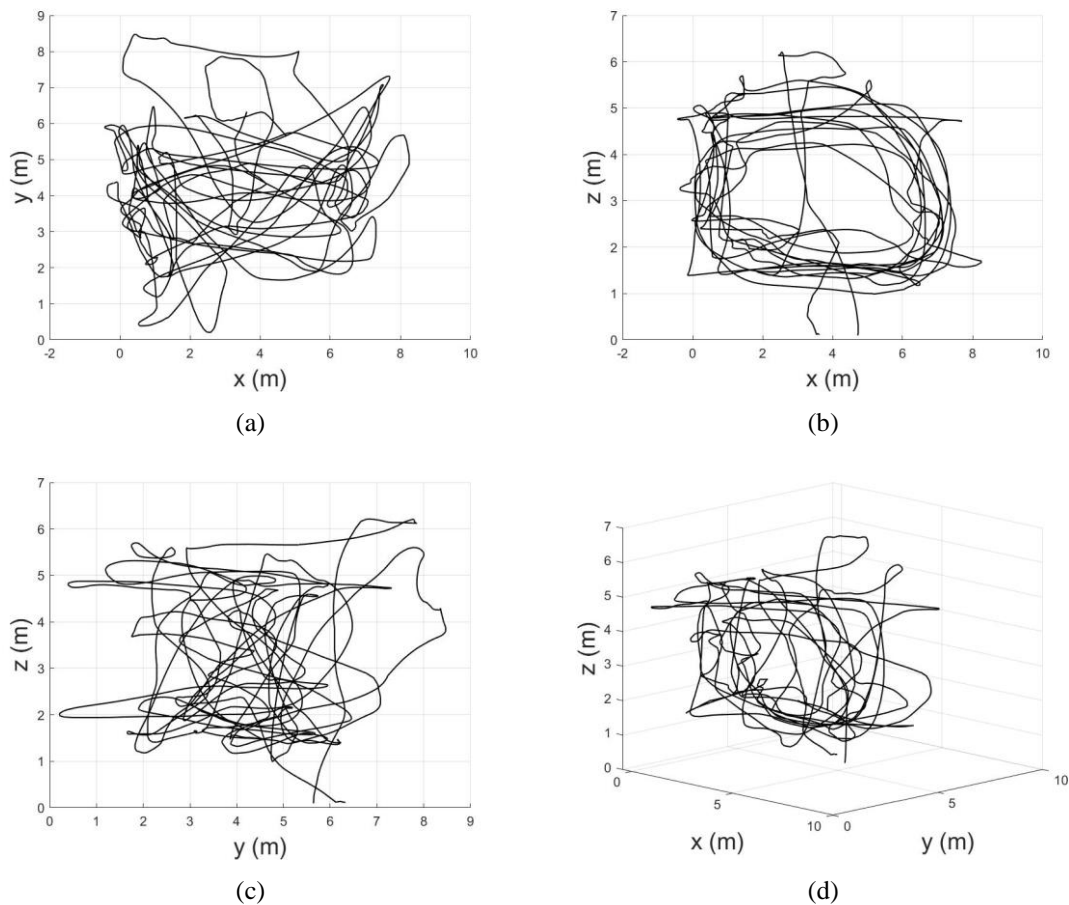


Figure 4.6 Set 3

In this flight, UAV flew circular path at an average speed of 0.87m/s. A total of 15899 UWB range and 44134 IMU data were measured. This data set has some 90-degree rapid and fast up-down movement. This data set is used for checking the accuracy difference for horizontal and vertical motion.

#### 4.4.4 Set 4 – Linear motion

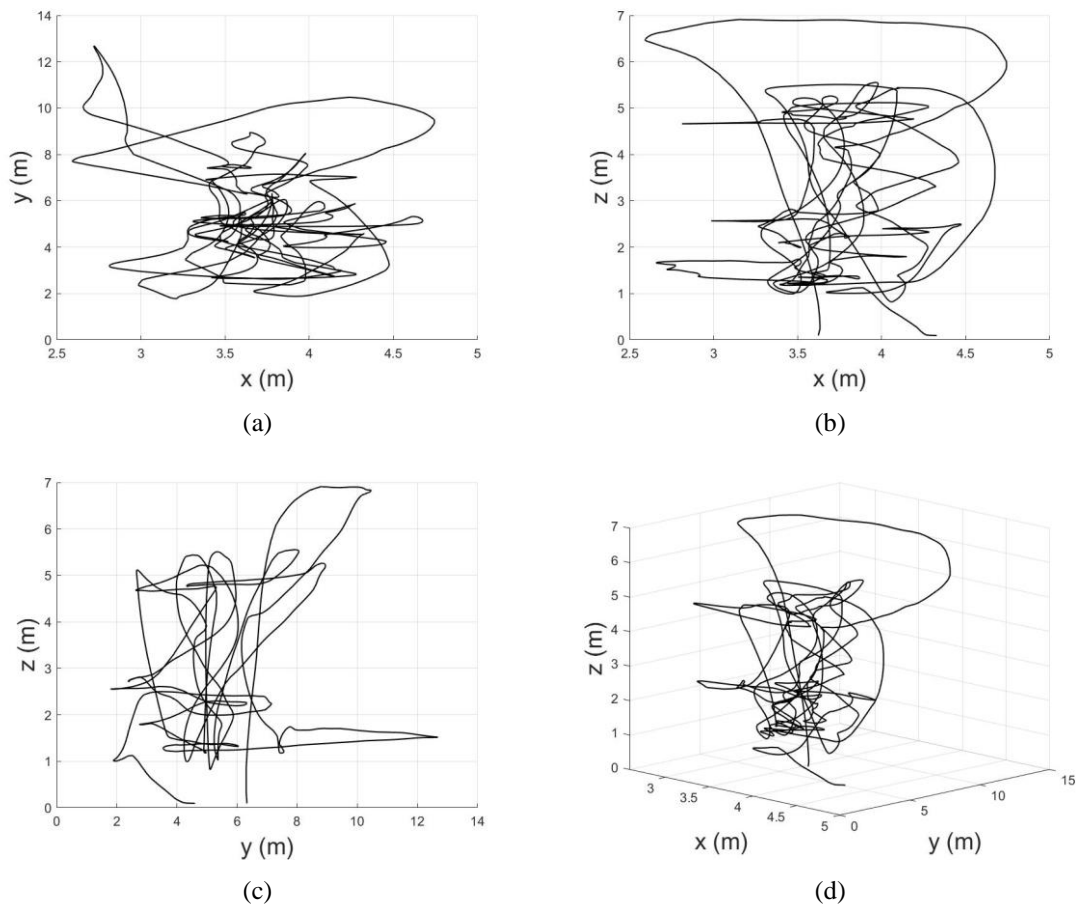


Figure 4.7 Set 4

In this flight, UAV flew linearly at an average speed of 0.82m/s. A total of 7958 UWB range and 22772 IMU data were measured. There is not much movement along the x-axis and mostly moved along the y-axis. Also, I can see two layers of linear path. This data is used to observe the accuracy change with height during linear motion.

#### 4.4.5 Set 5 –Complex motion

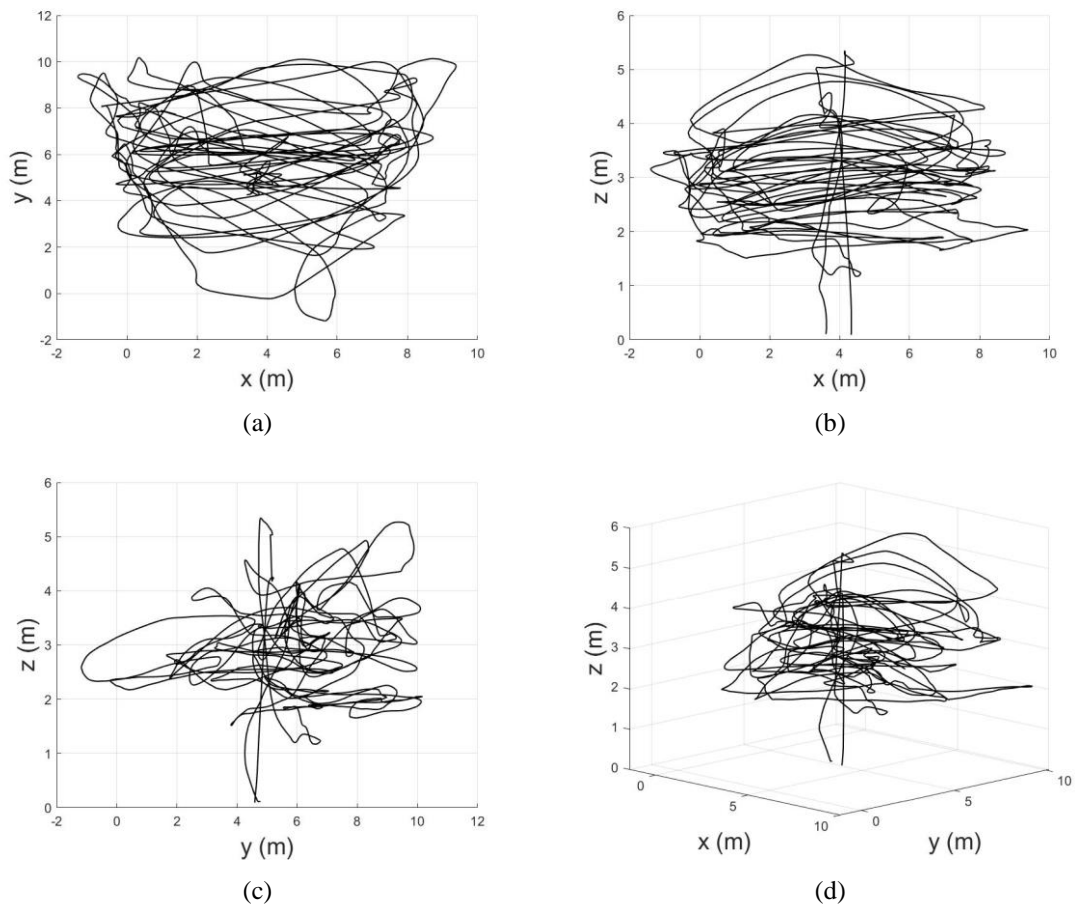


Figure 4.8 Set 5

In this flight, UAV flew randomly at a fast speed of 1.13m/s. A total of 16498 UWB range and 44413 IMU data were measured. This dataset represents the most complex and longest flight path. This dataset is used to test for accuracy changes that occur in fast motion.

## 4.5 Summary

In this chapter, I present the dataset I collected. First, the UAV platform and sensors are introduced. I used DJI Matrice 100 UAV platform with Intel NUC and TimeDomain P440 UWB in our study. Next, I demonstrated the experimental setup. Four UWB anchor is installed on the ground and UAV is tracked with the total station. After collecting data, I synchronize the time system between the ROS system and the total station. Total of five datasets was collected with different path and speed. These datasets are used for validation of our positioning algorithms in the next chapter. Also, I expect these data is used as benchmark dataset.

## **Chapter 5**

# **UWB based positioning with Multilateration**

### **5.1 Introduction**

In this chapter, the UWB based positioning system using multilateration in the GNSS-denied environment is proposed. The range-based positioning problem can be transformed into a graph problem that has high computational complexity. Therefore, it is necessary to use the numerical method, such as the multilateration method. Multilateration is the process that estimates the location of the target by measuring the distances of itself more than four anchor nodes whose positions are already known. However, flip ambiguity often occurs in multilateration, which causes huge positioning errors. In section 5.2, I describe what a flip ambiguity is and how it affects the positioning. In section 5.3, the multilateration method is described in three steps. Step 1 is to find an algebraic solution. Step 2 is correcting the solution under flip ambiguity. Step 3 is to refine the solution with non-linear optimization. In section 5.4, an experimental result is described. I summarize this chapter in section 5.5.

### **5.2 Flip ambiguity in multilateration**

Multilateration use distance measurement from UWB to calculate coordinates of the tag. Fundamental problem in multilateration is flip ambiguity which causes huge positioning error (W. Liu et al., 2016). Due to the error of the distance measurement, the estimated solutions also contains certain error. The solution is valid if the error of solution is

comparable to the ranging error. However, the estimated position error drastically increases compare to the ranging error due to an completely false position estimation. The reason of it is unsuitable geometric relations among the anchors. This phenomenon is called flip ambiguity which induces the most significant error.

Figure 5.1 shows the flip ambiguity in 2D spaces.  $A$ ,  $B$  and  $C$  are anchors located in known coordinates and  $T$  is tag to be estimated. In 2D multilateration, I can estimate the position of tag  $T$  when I have three ranging measurements from three anchors  $A$ ,  $B$  and  $C$  when they are located as Figure 5.1 (a). However, if three anchors are located in collinear space as Figure 5.1 (b), I can find two hypothesis  $T$  and  $T'$  which are symmetrical to the line  $ABC$  where  $T$  is correct solution and  $T'$  is flipped solution. Flip ambiguity also occurs if the anchors are nearly collinear as Figure 5.1 (c) due to an existence of ranging errors. There is a possibility to choose the wrong solution  $T'$  and it will cause a huge positioning error.

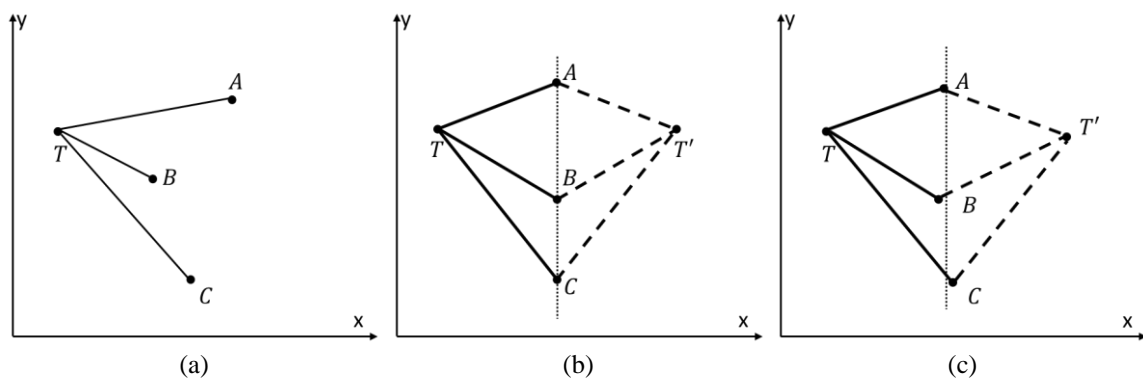


Figure 5.1 Flip ambiguity in 2D multilateration

Flip ambiguity also happens in 3D multilateration when a UWB tag with four UWB anchors that are almost coplanar, solution can be inverted into an incorrect solution that is

flipped over an anchor-formed plane. Figure 5.2 (a) shows how flip ambiguity occurs in 3D multilateration. I get two hypothesis  $T$  and  $T'$  which are symmetrical to the plane  $ABCD$  where  $T$  is correct solution and  $T'$  is flipped solution. In practical applications, UWB anchors are placed on tripods on the ground. To avoid flip ambiguity, the anchors are installed at different heights. However, due to a physical limitation of tripods, anchors often forms a shape close to a plane. Figure 5.2 (b) is a result of multilateration under flip ambiguity in experiment for dataset 1. As a result, estimated solution has huge error with negative. The next section introduces the multilateration method for correcting the flipped solutions.

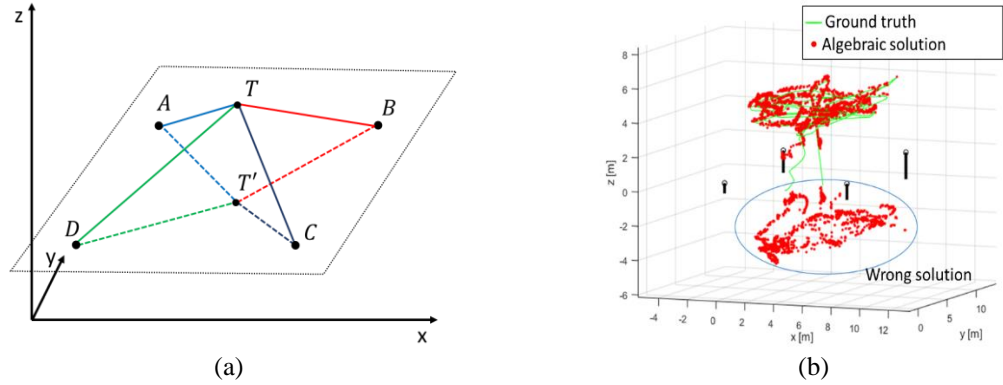


Figure 5.2 Flip ambiguity in 3D multilateration

### 5.3 Methodology

Here, I describe our method of multilateration under flip ambiguity. As shown in Figure 5.3, I suppose one UWB module is installed on UAV body and  $n$  UWB anchors are placed on the ground, where  $n \geq 3$ . The anchor frame can be set on an arbitrary location. The position of each UWB anchor in the anchor frame is assumed to be known in advance, where the

position of  $i$ th anchor in the anchor frame is denoted by  $\mathbf{x}_{ua}^i = [x_{ua}^i, y_{ua}^i, z_{ua}^i]$ . Through sequential communication between UWB module and each anchor, I get range data in which each data has different timestamp. Given the acquired data, I collect a set  $\mathbf{r} = \{r_1, r_2, \dots, r_m\}$  of range data for  $m$  different anchors, where  $3 \leq m \leq n$ . Only sets of range data acquired in a short time interval are used for the multilateration.

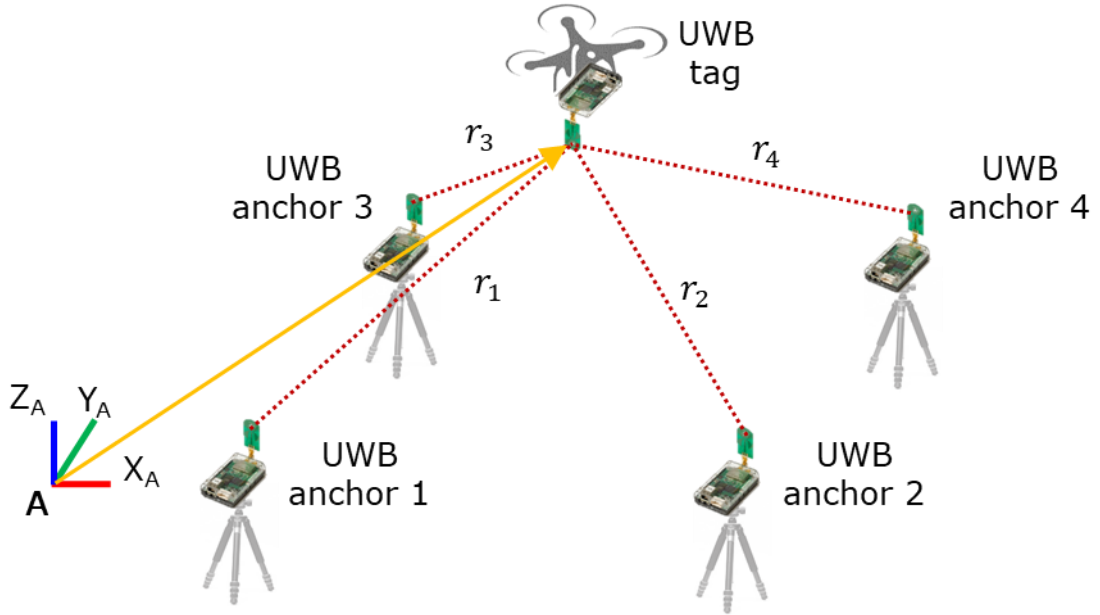


Figure 5.3 Description of UWB tag, UWB anchors and anchor frame.

The proposed multilateration algorithm consists of three major steps of (i) computation of an algebraic solution, (ii) correction of a solution by symmetric reflection through anchor plane and (iii) refinement of a solution using non-linear optimization, as described in Figure 5.4. Given one set of acquired range data  $\mathbf{r}$  and known position of anchors in the anchor frame, I first get an estimated position  $\mathbf{x}_{s1}$  of UWB module on UAV by computing algebraic solution. In the following step,  $\mathbf{x}_{s1}$  is corrected if it is considered flipped. The correction is

done by symmetric reflection of  $\mathbf{x}_{s1}$  through anchor plane formed by anchors. If  $\mathbf{x}_{s1}$  is not considered flipped, no correction is applied to  $\mathbf{x}_{s1}$ . Let  $\mathbf{x}_{s2}$  be a position produced by this step. In the last step,  $\mathbf{x}_{s2}$  is refined to  $\mathbf{x}_{s3}$  through non-linear optimization, where  $\mathbf{x}_{s3}$  is a final outcome of the proposed algorithm. I denote  $\mathbf{x}_{s3}$  by  $\mathbf{x}_{um} = [x_{um}, y_{um}, z_{um}]$ , which is the estimated position of the UWB module in the anchor frame.

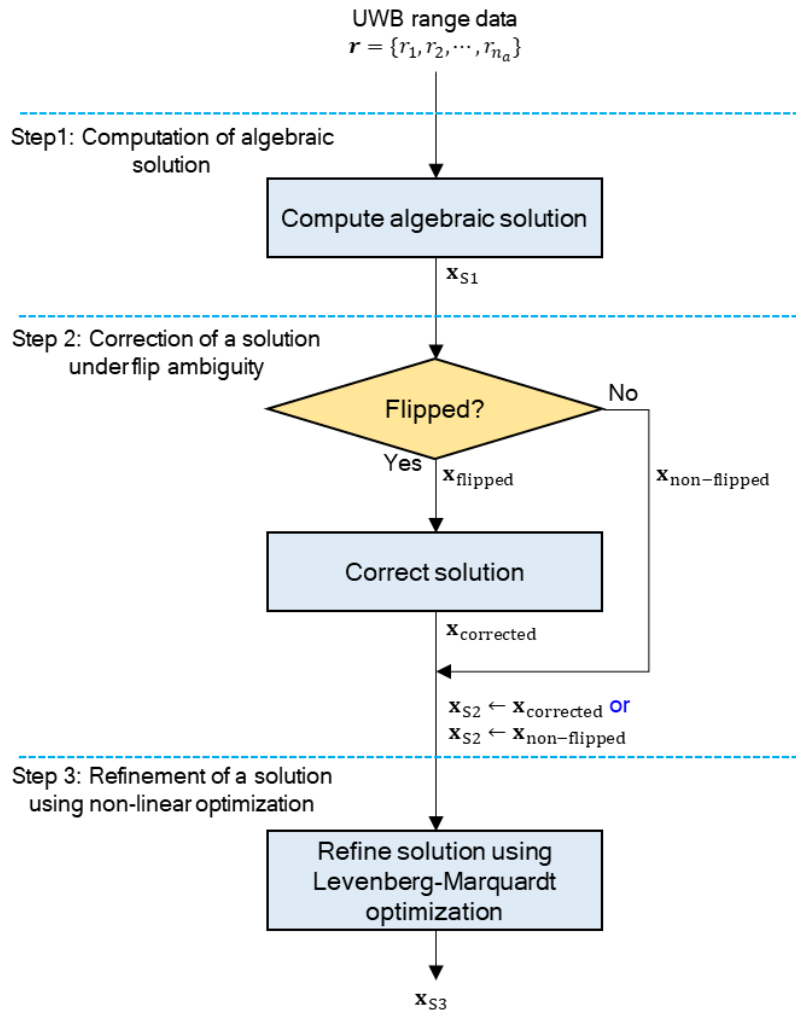


Figure 5.4 The proposed algorithm for multilateration, where it consists of major three steps producing initial estimated position, corrected position, and refined position, respectively.

### 5.3.1 Step 1 - Computation of an algebraic solution

In the first step, given one set of acquired range data  $\mathbf{r} = \{r_1, r_2, \dots, r_m\}$  and known position of anchors in the anchor frame, I get an estimated position  $\mathbf{x}_{s1} = [x_{s1}, y_{s1}, z_{s1}]$  of UWB module on UAV by computing algebraic solution. To do this, I adopted a method (Norrdine, 2012). From the equations

$$\|\mathbf{x}_{\text{um}} - \mathbf{x}_{\text{ua},i}\|_2^2 = r_i^2, \quad (5.1)$$

I get the linear system

$$A\mathbf{x}'_{\text{um}} = \mathbf{b}, \quad (5.2)$$

where

$$\mathbf{x}'_{\text{um}} = \begin{bmatrix} x_{\text{um}}^2 + y_{\text{um}}^2 + z_{\text{um}}^2 \\ x_{\text{um}} \\ y_{\text{um}} \\ z_{\text{um}} \end{bmatrix}, \quad (5.3)$$

$$A = \begin{bmatrix} 1 & -2x_{\text{ua},1} & -2x_{\text{ua},1} & -2x_{\text{ua},1} \\ 1 & -2x_{\text{ua},2} & -2x_{\text{ua},2} & -2x_{\text{ua},2} \\ \vdots & \vdots & \vdots & \vdots \\ 1 & -2x_{\text{ua},n_a} & -2x_{\text{ua},n_a} & -2x_{\text{ua},n_a} \end{bmatrix}, \quad (5.4)$$

$$\mathbf{b} = \begin{bmatrix} d_1^2 - x_{\text{ua},1}^2 - y_{\text{ua},1}^2 - z_{\text{ua},1}^2 \\ d_2^2 - x_{\text{ua},2}^2 - y_{\text{ua},2}^2 - z_{\text{ua},2}^2 \\ \vdots \\ d_{n_a}^2 - x_{\text{ua},n_a}^2 - y_{\text{ua},n_a}^2 - z_{\text{ua},n_a}^2 \end{bmatrix}. \quad (5.5)$$

Then, I get the solution candidates by recursive least squares.

$$\mathbf{x}'_{\text{um}} = (A^T A)^{-1} A^T \mathbf{b} \quad (5.6)$$

Among the solution candidates, I choose one that minimizes

$$\sum_i (r_i - \|\mathbf{x}_{um} - \mathbf{x}_{ua,i}\|_2)^2. \quad (5.7)$$

as an outcome of this step.

### 5.3.2 Step 2 - Correction of a Solution by Symmetric Reflection through Anchor Plane under Flip Ambiguity

When  $m$  anchors for the range data form a plane or a near-plane, it occurs a geometric ambiguity in estimating  $\mathbf{x}_{s1}$ . Due to the geometric ambiguity called *flip ambiguity*, two strong solution candidates for  $\mathbf{x}_{s1}$  exist, leading to frequent creation of  $\mathbf{x}_{s1}$  having incorrect flipped solution in the previous step. Thus,  $\mathbf{x}_{s1}$  should be corrected if it is considered flipped by the flip ambiguity.

In this work, I consider a ground-based anchor system where each anchor is usually installed using a tripod on a flat ground, which is commonly used in many real operation cases. In the ground-based anchor system, I assume (i) the anchor-to-anchor distance is often much larger than height difference between anchors, and (ii) anchors are located by a tripod near the ground, so that UAV flying height is often larger than the anchor height on the ground. These two assumptions hold in many real cases. Under these conditions, an anchor plane formed by anchors can be considered almost parallel to the ground, and it is located near the ground. Hence, I consider  $\mathbf{x}_{s1}$  flipped if  $z_{s1} < T_z$ , where I used  $T_z = 0$  indicating the height of ground. By this rule,  $\mathbf{x}_{s1}$  is classified into 'flipped' ( $\mathbf{x}_{\text{flipped}}$ ) or 'non-flipped'

( $\mathbf{x}_{\text{non-flipped}}$ ), as described in Figure 5.5  $\mathbf{x}_{\text{flipped}}$  is corrected to a new solution  $\mathbf{x}_{\text{corrected}}$ , while  $\mathbf{x}_{\text{non-flipped}}$  is used without correction for subsequent non-linear optimization step.

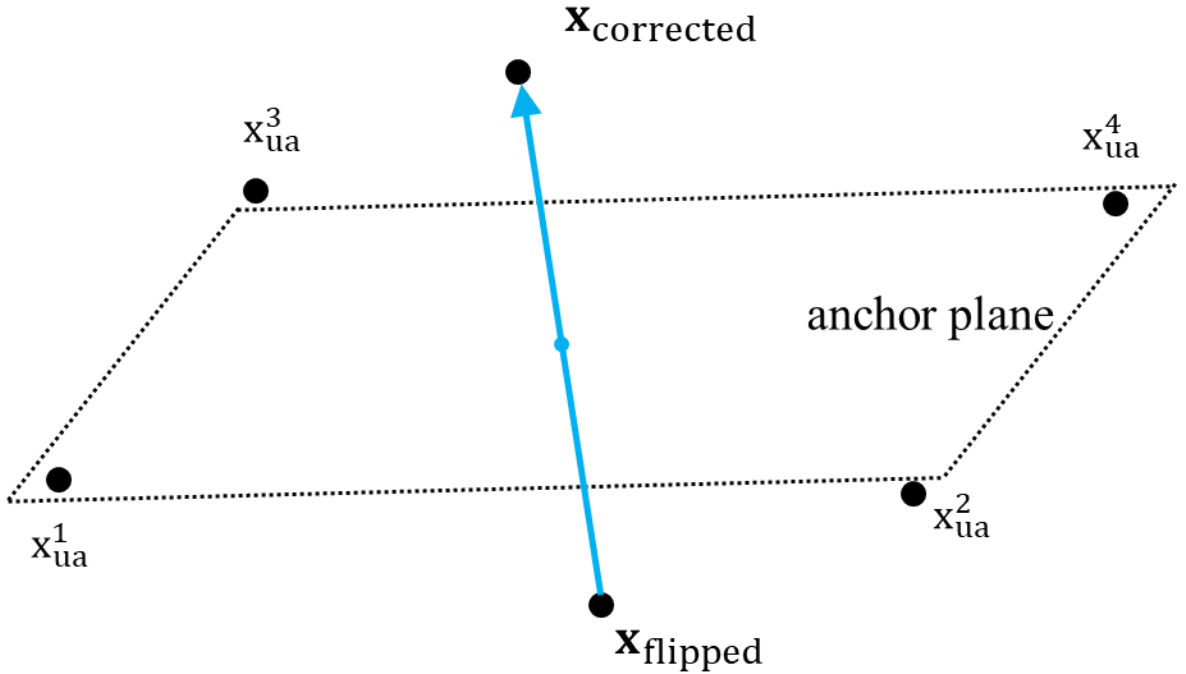


Figure 5.5 Symmetric reflection of a flipped solution through anchor plane

The correction is done by symmetric reflection of  $\mathbf{x}_{\text{flipped}}$  through the anchor plane, as the flip ambiguity produces ambiguity symmetrically with respect to the anchor plane. Figure 4 describes how I correct  $\mathbf{x}_{\text{flipped}}$  to  $\mathbf{x}_{\text{corrected}}$ . First, I model anchor plane by the equation  $ax + by + cz + 1 = 0$ . The plane parameter  $\mathbf{p}_{\text{ap}} = [a, b, c]^T$  can be obtained by solving the linear system  $A_{\text{ap}}\mathbf{p}_{\text{ap}} = \mathbf{b}_{\text{ap}}$ , where

$$A_{ap} = \begin{bmatrix} x_{ua}^1 & y_{ua}^1 & z_{ua}^1 \\ x_{ua}^2 & y_{ua}^2 & z_{ua}^2 \\ \vdots & \vdots & \vdots \\ x_{ua}^m & y_{ua}^m & z_{ua}^m \end{bmatrix} \quad (5.8)$$

and

$$\mathbf{b}_{ap} = -\mathbf{1}_{m \times 1}. \quad (5.9)$$

Then,  $\mathbf{x}_{flipped}$  is corrected to  $\mathbf{x}_{corrected}$  by

$$\mathbf{x}_{corrected} = \mathbf{x}_{flipped} - 2 \cdot (\mathbf{p}_{ap} / \|\mathbf{p}_{ap}\|) \cdot \mathbf{v} \quad (5.10)$$

where  $\mathbf{v} = (ax + by + cz + 1) / \|\mathbf{p}_{ap}\|$ . I denote  $\mathbf{x}_{corrected}$  or  $\mathbf{x}_{non-flipped}$  by  $\mathbf{x}_{s2}$  as an outcome of this step.

### 5.3.3 Step 3 - Refinement of a solution using non-linear optimization

The last step is to refine the solution using non-linear optimization. I refine  $\mathbf{x}_{s2}$  to  $\mathbf{x}_{s3}$  by solving

$$\hat{\mathbf{x}}_{s3} = \arg \min_{\mathbf{x}_{s3}} \sum_i e_i^2 \quad (5.11)$$

where  $e_i = r_i - \|\mathbf{x}_{s3} - \mathbf{x}_{ua}^i\|_2$ . Here,  $\mathbf{x}_{s2}$  is used as initial value in the optimization. I used the Levenberg-Marquardt algorithm (Davis, 1993) for this optimization. As a result of this optimization, I get  $\mathbf{x}_{s3}$  which is a final outcome of our algorithm.

## 5.4 Experimental results

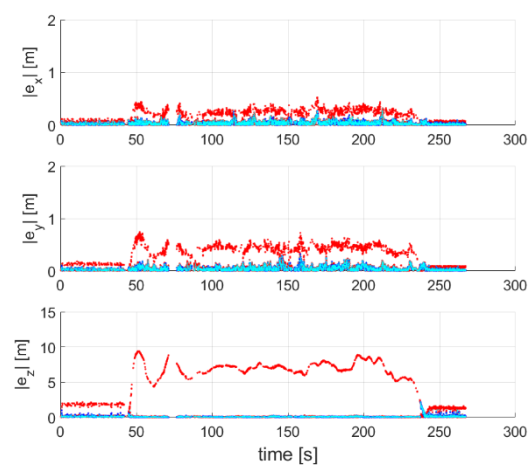
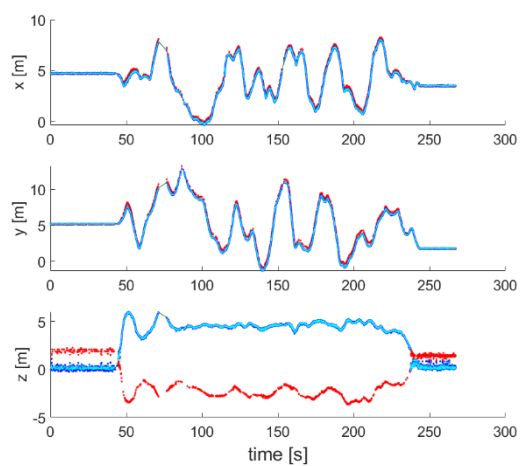
Given the acquired data described in chapter 4, I collected sets of range data for four anchors. I applied our multilateration algorithm to range set only acquired in a short time interval. I used 0.1 seconds as a threshold of time interval. As a result, our experiments achieved the multilateration results from only 15.95% of total time steps in the dataset. I use mean absolute error (MAE) to measure the positioning error.

Table 5.4 describes MAE of each step. After step 1, I get 1.289m of MAE in average due to flip ambiguity. Step 2 decrease MAE significantly by correcting flip ambiguity from 1.289m to 0.133m. Step3 decrease MAE by 0.008m from 0.133m to 0.125m.

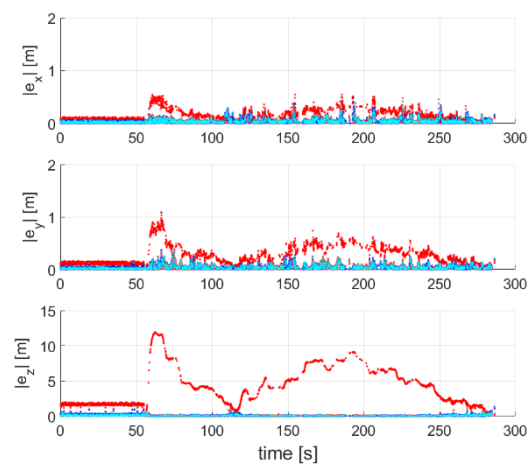
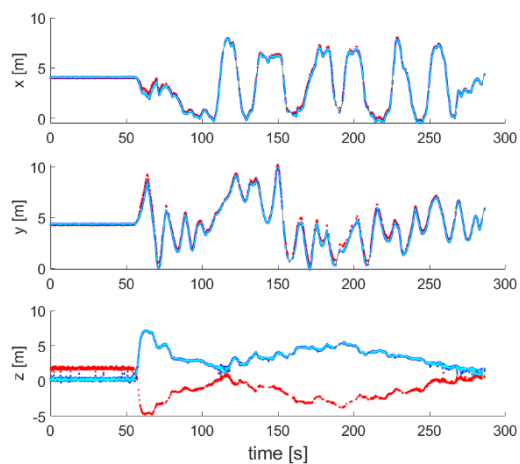
Z-axis accuracy and overall accuracy were the best at step 3 for all the data sets.

Table 5.4 Multilateration results for each step

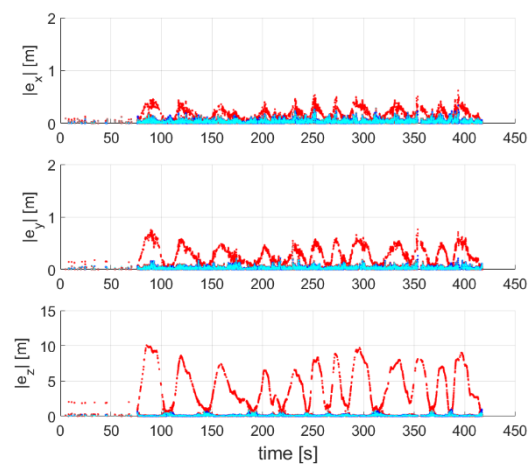
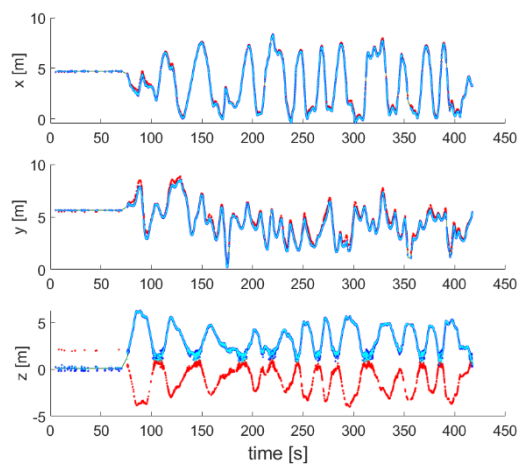
Methods	Position	Set 1	Set 2	Set 3	Set 4	Set 5	Mean
$X_{S1}$	x	0.081	0.076	0.076	0.055	0.089	0.075
	y	0.121	0.113	0.097	0.084	0.110	0.105
	z	1.463	1.314	1.250	0.915	1.364	1.261
	xyz	1.494	1.343	1.273	0.938	1.396	1.289
$X_{S2}$	x	0.038	0.042	0.041	0.033	0.058	0.043
	y	<b>0.044</b>	0.044	0.031	0.041	0.038	0.040
	z	0.086	0.098	0.095	0.124	0.095	0.099
	xyz	0.122	0.134	0.122	0.151	0.137	0.133
$X_{S3}$	x	<b>0.037</b>	<b>0.041</b>	<b>0.040</b>	<b>0.031</b>	<b>0.057</b>	<b>0.041</b>
	y	<b>0.044</b>	<b>0.043</b>	<b>0.030</b>	<b>0.040</b>	<b>0.037</b>	<b>0.039</b>
	z	<b>0.079</b>	<b>0.089</b>	<b>0.084</b>	<b>0.118</b>	<b>0.087</b>	<b>0.091</b>
	xyz	<b>0.114</b>	<b>0.125</b>	<b>0.112</b>	<b>0.145</b>	<b>0.129</b>	<b>0.125</b>



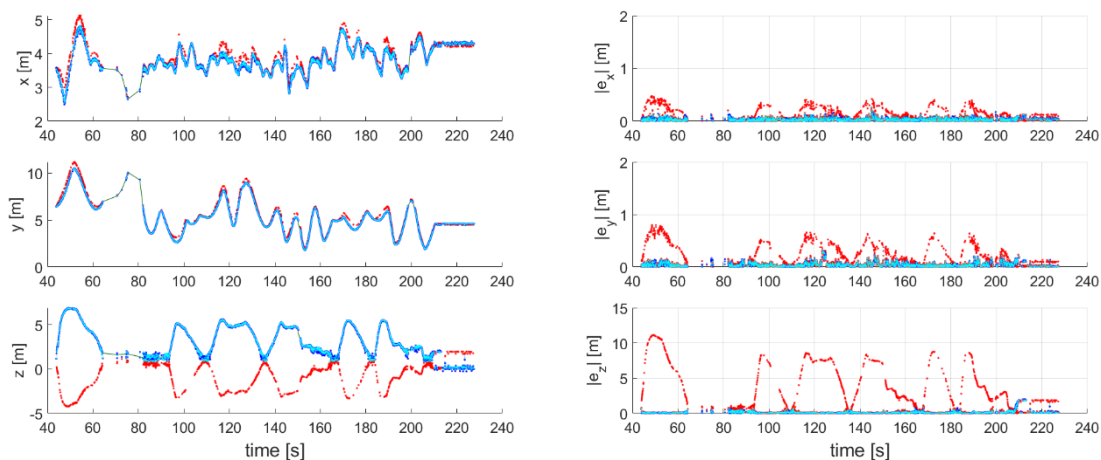
Set 1



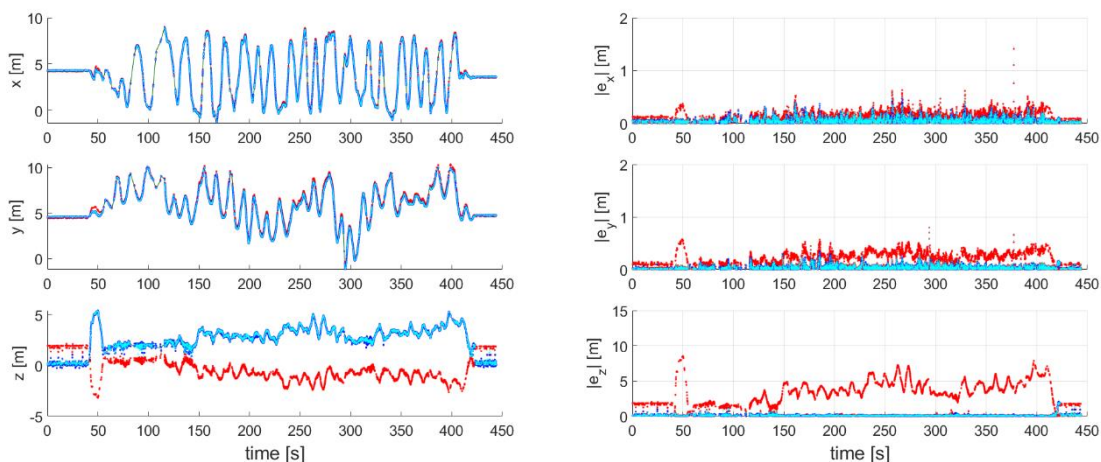
Set 2



Set 3



Set 4



Set 5

Figure 5.6 Ground-truth trajectory and estimated position (left column) and absolute error (right column) over time. Green: Ground truth, red: step 1, blue: step 2, cyan: step 3.

Figure 5.6 shows the results of each step for 5 data sets. Green lines represent the ground truth, red dots represent the result of step 1, blue dots represent result of step 2 and cyan dots represent result of step 3. The effect of each step is analyzed in the following sections.

### 5.4.1 Error Analysis in Algebraic Solution

Figure 5.7 shows error in algebraic solution  $\mathbf{x}_{s1}$  by (Norrdine, 2012). To see the error by flip ambiguity, I separately present errors in  $\mathbf{x}_{\text{flipped}}$  and  $\mathbf{x}_{\text{non-flipped}}$ . I could see huge error in  $\mathbf{x}_{\text{flipped}}$  caused by flip ambiguity, especially in z-axis. From this result, I found that algebraic solution such as (Norrdine, 2012) can produce severely erroneous solution by flip ambiguity.

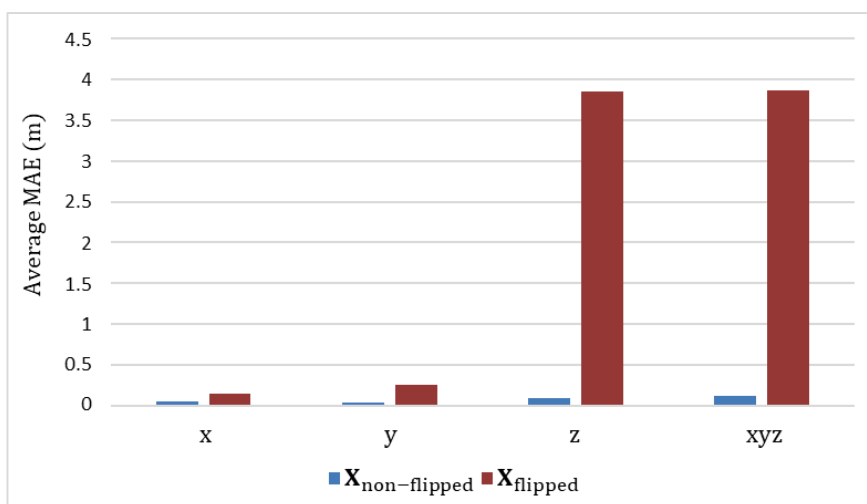


Figure 5.7 Step 1 Average MAE of 5 data sets

### 5.4.2 Effect of the Proposed Correction under Flip Ambiguity

Figure 5.8 shows the effect of proposed correction method under flip ambiguity. Note that  $\mathbf{x}_{\text{flipped}}$  is corrected to  $\mathbf{x}_{\text{corrected}}$  by the proposed correction method. As indicated by errors in  $\mathbf{x}_{\text{flipped}}$  and  $\mathbf{x}_{\text{corrected}}$ , the errors by flip ambiguity were significantly reduced by the proposed correction method which is symmetric reflection through anchor plane.

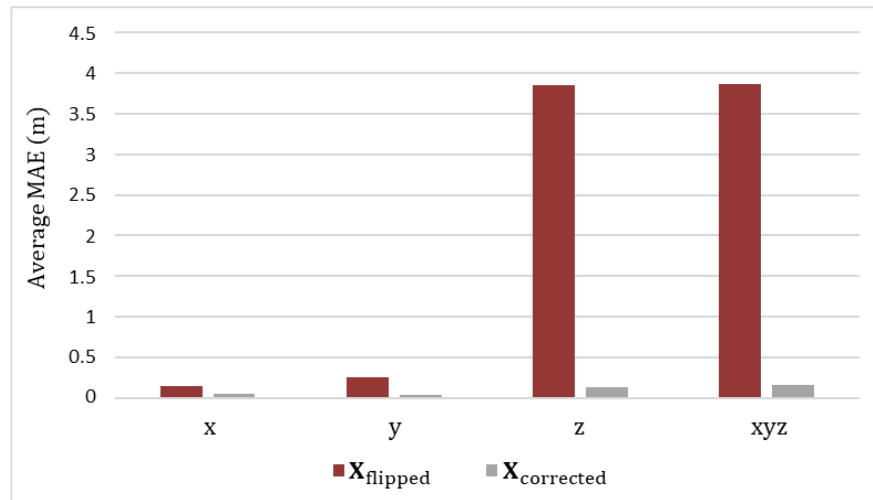


Figure 5.8 Step 2 Average MAE of 5 data sets

### 5.4.3 Effect of Solution Refinement by Non-linear optimization

Figure 5.9 shows the effect of solution refinement by Levenberg-Marquardt non-linear optimization. Note that  $x_{s2}$  is refined to  $x_{s3}$ , and it showed that non-linear optimization slightly enhanced the accuracy in position estimation.

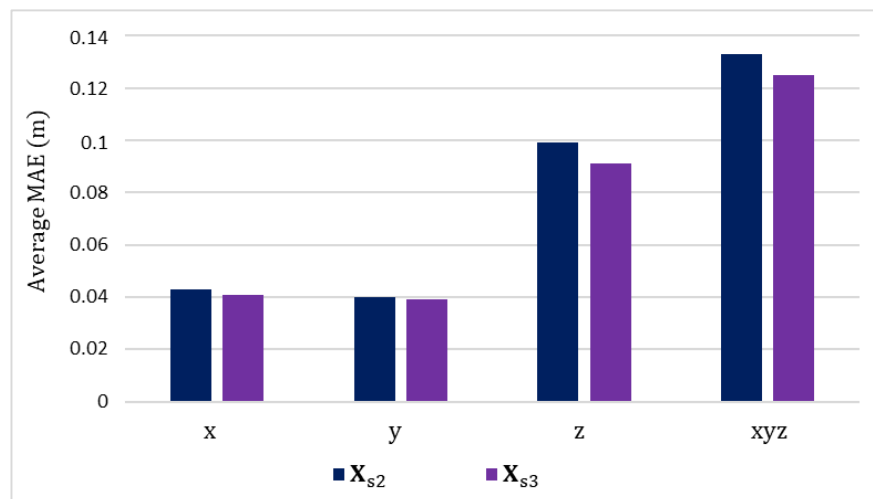


Figure 5.9 Step 3 Average MAE of 5 data sets

## 5.5 Summary

In this chapter, I presented a method for multilateration under the flip ambiguity for UAV positioning using UWB. The proposed multilateration algorithm initially computed an algebraic solution through recursive least squares. If the initially estimated position was considered flipped by the flip ambiguity, then the position was corrected by symmetric reflection of the position through the anchor plane. Lastly, the estimated position was refined by non-linear optimization. Through experiments in a real environment, I demonstrated that the developed algorithm effectively resolved the issue of flip ambiguity, leading to significant improvement of the accuracy in position estimation.

## **Chapter 6**

# **EKF based UAV Positioning Algorithm**

### **6.1 Introduction**

In the previous chapter, I used multilateration as a method of UWB positioning. However, multilateration could only be used when observations were made from four anchors in a short time. As a result, UAV was not continuously estimated in all intervals. To solve this problem, this chapter performed positioning using Extended Kalman Filter (EKF). EKF is a filtering method that can make accurate predictions based on the measurements from various sensors. This property allows us to fuse IMU to UWB data for improving accuracy. In this chapter, I develop UWB-IMU positioning with EKF. In section 6.2, general EKF algorithm and our motion model is described. In section 6.3, experimental result is described. Discussions for the results are in section 6.4.

### **6.2 Kalman Filter**

A Kalman filter estimates the new state of a process in two steps. The first step is a time update, also called a prediction. The new state of the process is estimated by previous states with control inputs. The second step is measurement update, also called as the correction. Measurement is used to correct estimated states at the prediction step.

### 6.2.1 Process model

A Kalman filter explains the procedure using two linear models. The first model represents the relation between the state in current time step and the state in previous time step with control inputs and transition noise. The transition model is expressed as

$$\mathbf{x}_k = A\mathbf{x}_{k-1} + B\mathbf{u}_k + \mathbf{w}_k \quad (6.1)$$

where  $\mathbf{x}_k$  is the state vector of the process in the  $k$ th time interval. Matrix  $A$  describes the relation of two successive states without the control input and transition noise.  $\mathbf{u}_k$  is the control input of the system in the  $k$ th time interval and  $B$  relates the effect of control input. Finally,  $\mathbf{w}_k$  is a zero mean Gaussian noise with covariance  $Q$ . Observation model relates the measurement and the new state as

$$\mathbf{z}_k = H\mathbf{x}_k + \mathbf{v}_k \quad (6.2)$$

where  $\mathbf{z}_k$  is the noisy measurement vector in the  $k$ th time interval,  $H$  is a matrix that relates state with measurements and  $\mathbf{v}_k$  is the measurement noise which has zero mean Gaussian noise with covariance  $R$ . Two fundamental assumptions in Kalman filter are as follows: (1) state transitions and the observation vectors are linear and (2) the transition noise and measurement noise are zero mean white Gaussian.

## 6.2.2 Equations

Kalman filter has two steps: prediction and correction. The prediction step gives an a priori estimate of the new state,  $\tilde{x}_k$ , based on information prior to the  $k$ th measurement. The prediction step is represented as (adapted from (Welch & Bishop, 1995)):

$$\tilde{x}_k = A\hat{x}_{k-1} + Bu_k \quad (6.3)$$

where  $\hat{x}_{k-1}$  is the final estimate (a posteriori estimate) at the  $(k-1)$ th time interval. In the correction step, the posteriori estimate is computed as

$$\hat{x}_k = \tilde{x}_k + M_k(z_k - H\tilde{x}_k) \quad (6.4)$$

Where

$$M_k = \tilde{P}_k H^T (H \tilde{P}_k H^T + R)^{-1}, \quad (6.5)$$

$$\tilde{P}_k = A \hat{P}_k A^T + Q, \quad (6.6)$$

$$\hat{P}_k = (1 - M_k H) \tilde{P}_k. \quad (6.7)$$

A useful observation from equation (6.4) is that a posteriori estimate is the addition of the a priori estimate and a weighted difference between the measurement and predicted measurement. Note that in equation (6.5) for  $M_k$  I observe that if the measurement error  $R$  approaches zero,  $M_k$  becomes  $H^{-1}$ , and the a posteriori estimate,  $\hat{x}_k$ , is  $H^{-1} z_k$ . In other words, due to the high accuracy of the measurement, I do not use the a priori estimate. On the other

hand, if  $R$  becomes significantly larger,  $M_k$  approaches zero and the a posteriori estimate is equal to the a priori estimate.

### 6.2.3 Extended Kalman Filter (EKF)

Kalman filter addresses the general problem which is governed by linear equation. However, the process to be estimated and observation equations are non-linear relationship in many cases. The EKF is a Kalman filter that linearizes the nonlinear models around the current value of the state vector. The general equations for nonlinear process and observation models are as follows (Bishop & Welch, 2001):

$$x_k = f(x_{k-1}, u_k, w_{k-1}) \quad (6.8)$$

$$z_k = h(x_k, v) \quad (6.9)$$

where  $w$  is the process noise with covariance matrix  $Q$  and  $v$  is the measurement noise with covariance matrix  $R$  and  $u_k$  is the input to the system. The extended Kalman filter uses multivariate Taylor Series expansions with the Jacobian matrix of each nonlinear function to linearize the model at a specific point. Equation (6.8) and (6.9) are linearized as follows:

$$x_k \approx \tilde{x}_k + A(x_{k-1} - \hat{x}_{k-1}) + Ww_{k-1} \quad (6.10)$$

$$z_k = \tilde{z}_k + H(x_k - \tilde{x}_k) + Vv_k \quad (6.11)$$

An approximate state vector and an approximate observation vector without error are expressed as follows.

$$\tilde{x}_k = f(\hat{x}_{k-1}, u_k, 0) \quad (6.12)$$

$$\tilde{z}_k = h(\tilde{x}_k, 0) \quad (6.13)$$

Where  $\hat{x}_{k-1}$  is the a posteriori estimate of the state vector computed from a previous time step, H and A are the Jacobian matrices of  $h$  and  $f$  functions as follows:

$$A_{[i,j]} = \frac{\partial f_{[i]}}{\partial x_{[j]}}(\hat{x}_{k-1}, u_k, 0) \quad (6.14)$$

$$H_{[i,j]} = \frac{\partial h_{[i]}}{\partial x_{[j]}}(\tilde{x}_k, 0) \quad (6.15)$$

V and W are the Jacobian matrices of  $h$  and  $f$  with respect to  $v$  and  $w$ :

$$W_{[i,j]} = \frac{\partial f_{[i]}}{\partial w_{[j]}}(\hat{x}_{k-1}, u_k, 0) \quad (6.16)$$

$$V_{[i,j]} = \frac{\partial h_{[i]}}{\partial v_{[j]}}(\tilde{x}_k, 0) \quad (6.17)$$

By applying Kalman Filter to the linearized equations (6.10) and (6.11), a posteriori estimate of the state vector is computed as follows:

$$\hat{x}_k = \tilde{x}_k + K_k(z_k - f(\tilde{x}_k, 0)) \quad (6.18)$$

where the Kalman gain matrix  $K_k$  is computed as follows:

$$K_k = \tilde{P}_k H_k^T (H_k \tilde{P}_k H_k^T + V_k R V_k^T)^{-1} \quad (6.19)$$

the error covariance matrix  $P$  is defined as follows:

$$\tilde{P}_k = A \hat{P}_{k-1} A + W Q_{k-1} W^T \quad (6.20)$$

and

$$\hat{P}_k = (I - K_k H_k) \tilde{P}_k. \quad (6.21)$$

Figure 6.1 shows complete picture of the operation of the EKF.

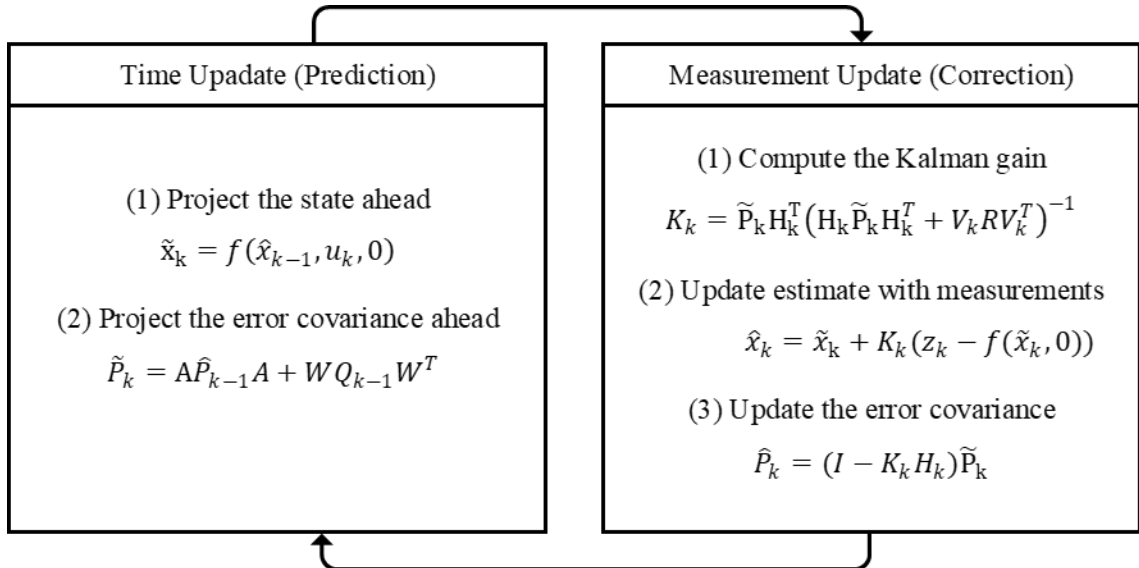


Figure 6.1 A complete picture of the operation of the extended Kalman filter

### 6.3 IMU driven motion model and measurement model

UAVs usually use IMU based on microelectromechanical systems(MEMS) to control postures so IMU observations are available to fuse with UWB based positing. The inertial measurement unit (IMU) consists of accelerometers, gyroscopes, and sometimes magnetometers (Ruan & Balch, 2018). Using IMU information, the physical model can be applied to improve the accuracy of each state prediction. However, IMUs typically suffer from accumulated error so that additional sensor is required to calibrate the drift as mentioned in chapter 2. By applying EKF, IMU and UWB can be combined to correct the drift and to make more accurate predictions. I apply IMU-driven motion model to apply EKF as follows.

IMU measurements of acceleration  $A^s$  and angular rates  $W^s$  are taken as control signals in the sense that they are used to predict the future pose of the UAV. Since IMU has drift error, I estimate drifted bias at each state. I estimate 3D Linear velocity of the UAV  $V$ , 3D bias of accelerometers  $A^b$ , 3D bias of gyroscopes  $W^b$ , 3D coordinates of the UAV  $B$  and 3D pose of the UAV  $q$ . Process noise of control are 3D velocity perturbation impulses  $\varepsilon_V$ , 3D rotation perturbation impulses  $\varepsilon_q$ , 3D random walks of accelerometer biases  $\varepsilon_{A^b}$  and 3D random walks of gyroscope biases  $\varepsilon_{W^b}$ . I can set state vector  $x$ , control vector  $u$  and error vector  $\varepsilon$  as follows.

$$x = \begin{bmatrix} V \\ A^b \\ W^b \\ B \\ q \end{bmatrix}, \quad (6.21)$$

$$\mathbf{u} = \begin{bmatrix} A^S \\ W^S \end{bmatrix}, \quad (6.22)$$

$$\boldsymbol{\varepsilon} = \begin{bmatrix} \varepsilon_V \\ \varepsilon_q \\ \varepsilon_{A^b} \\ \varepsilon_{W^b} \end{bmatrix} \quad (6.23)$$

I can formulate transition function as follows.

$$\mathbf{x}_t = f(\mathbf{x}_t, \mathbf{u}_t, \boldsymbol{\varepsilon}_t) = \begin{bmatrix} V_{t-1} + \left( R_{q_{t-1}} (A_t^S + A_{t-1}^b + \varepsilon_{A^b}) \right) \Delta t + \varepsilon_V \\ A_{t-1}^b + \varepsilon_{A^b} \\ W_{t-1}^b + \varepsilon_{W^b} \\ B_{t-1} + (V_{t-1} + \varepsilon_V) \Delta t + \frac{1}{2} \left( R_{q_{t-1}} (A_t^S + A_{t-1}^b + \varepsilon_{A^b}) \right) \cdot (\Delta t)^2 \\ q_{t-1} \otimes q \{ (W_t^S + W_{t-1}^b + \varepsilon_{W^b}) \Delta t + \varepsilon_q \} \end{bmatrix} \quad (6.24)$$

Measurement equation of range measurement from  $i$ th anchor is

$$z_t = h(\mathbf{x}_t, v_t) = \sqrt{(x_k - s_{x,i})^2 + (y_k - s_{y,i})^2 + (z_k - s_{z,i})^2} + v_t. \quad (6.25)$$

By applying EKF in this model, I can achieve EKF based positioning. Each time IMU measurements are accepted, predictions are made through a transition function. Also, each time UWB measurements are accepted, corrections are made through a measurement equation by EKF.

## 6.4 Experimental Results using EKF Methods

### 6.4.1 Overview of the positioning results

I perform EKF for our dataset described in chapter 4. In contrast to multilateration which achieved results from only 15.95% of total time steps in the dataset, I got result continuously from all time step for EKF. I use mean absolute error (MAE) to measure the positioning error.

Table 6.1 shows MAE of each dataset. Mean value of MAE in xyz for five data set is 0.103m. EKF performs better in all the datasets. For x and y axis, EKF performs 0.005m and 0.004m better than multilateration. For z axis, EKF performs 0.017m better than multilateration. The main reason of it is that EKF allows us to fuse IMU measurement with UWB measurement. Especially, accuracy of z axis improved much more than x and y axis.

Table 6.1 EKF and multilateration results

Methods	Position	Set 1	Set 2	Set 3	Set 4	Set 5	Mean
EKF	x	<b>0.029</b>	<b>0.037</b>	<b>0.034</b>	<b>0.025</b>	<b>0.055</b>	<b>0.036</b>
	y	<b>0.034</b>	<b>0.041</b>	0.032	<b>0.034</b>	<b>0.034</b>	<b>0.035</b>
	z	<b>0.055</b>	<b>0.078</b>	<b>0.082</b>	<b>0.084</b>	<b>0.069</b>	<b>0.074</b>
	xyz	<b>0.083</b>	<b>0.110</b>	<b>0.107</b>	<b>0.106</b>	<b>0.111</b>	<b>0.103</b>
multilateration (step 3)	x	0.037	0.041	0.040	0.031	0.057	0.041
	y	0.044	0.043	<b>0.030</b>	0.040	0.037	0.039
	z	0.079	0.089	0.084	0.118	0.087	0.091
	xyz	0.114	0.125	0.112	0.145	0.129	0.125

Figure 6.2~6.6 shows ground-truth trajectory and estimated positions. I divided flight trajectory into twelve sections from takeoff to landing and displayed with estimated positions. Figure 6.7 summarizes the positioning error over time for all the datasets.

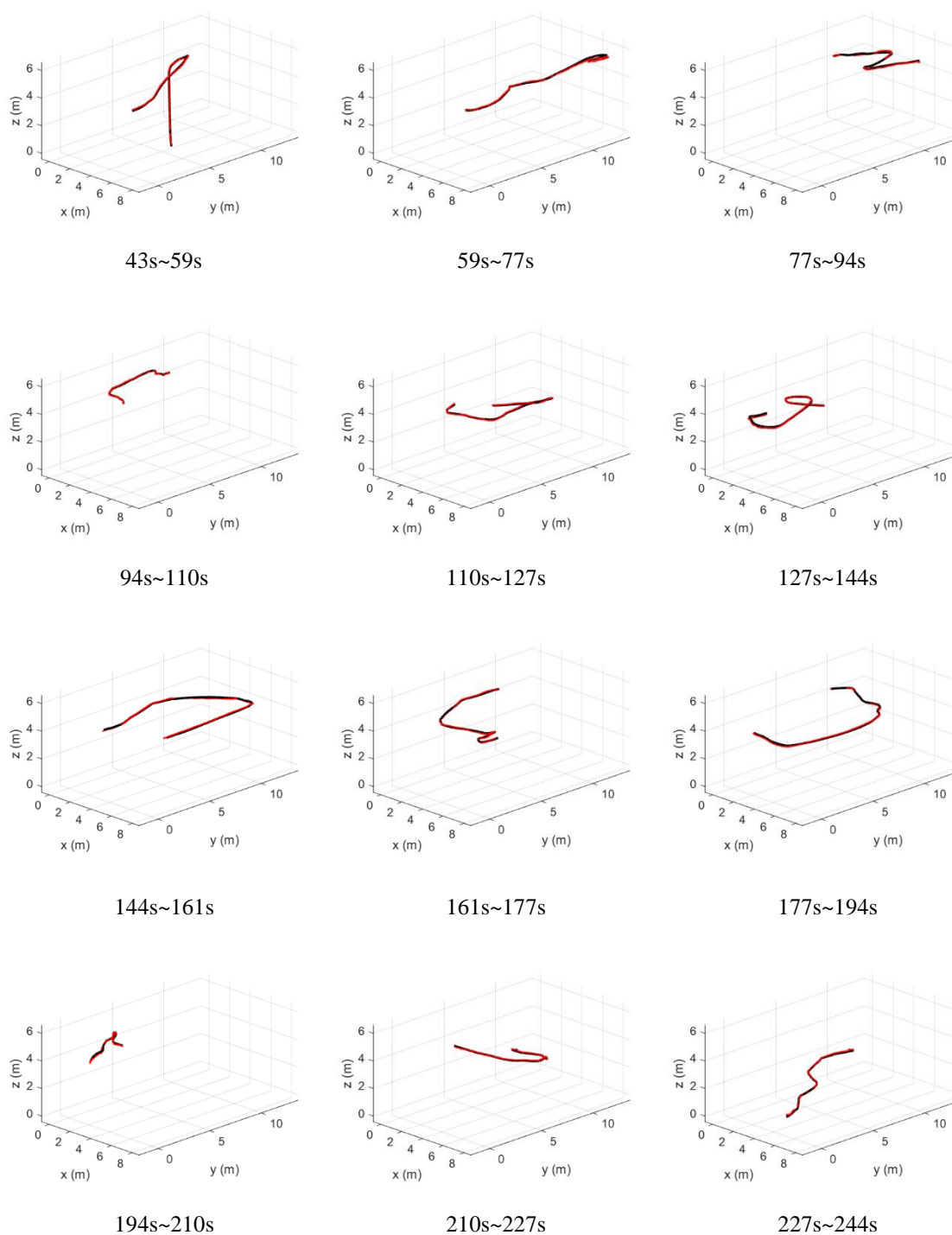


Figure 6.2 Set 1 - ground-truth trajectory(Black) and estimated position(Red) in 3D space.

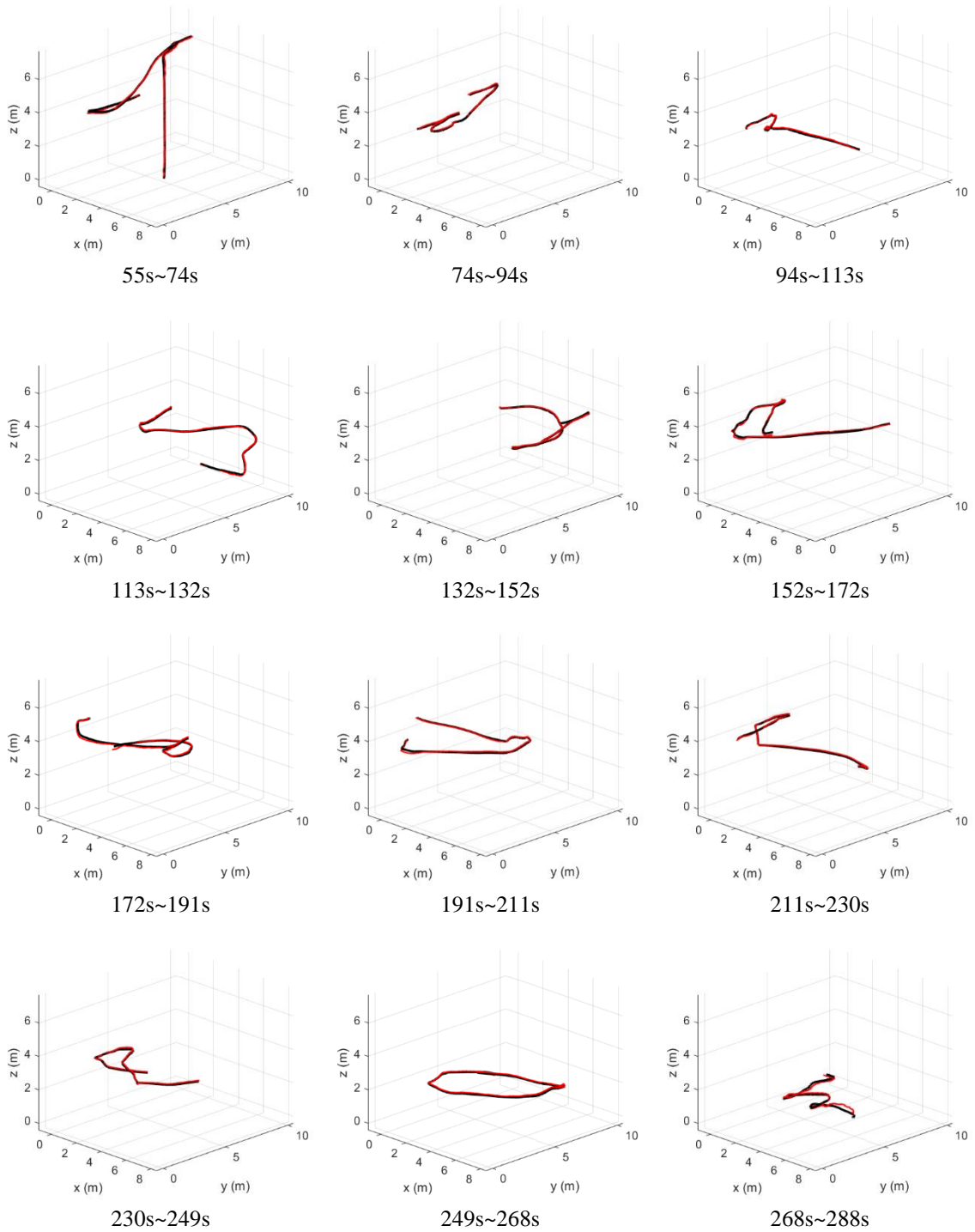


Figure 6.3 Set 2 - ground-truth trajectory(Black) and estimated position(Red) in 3D space.

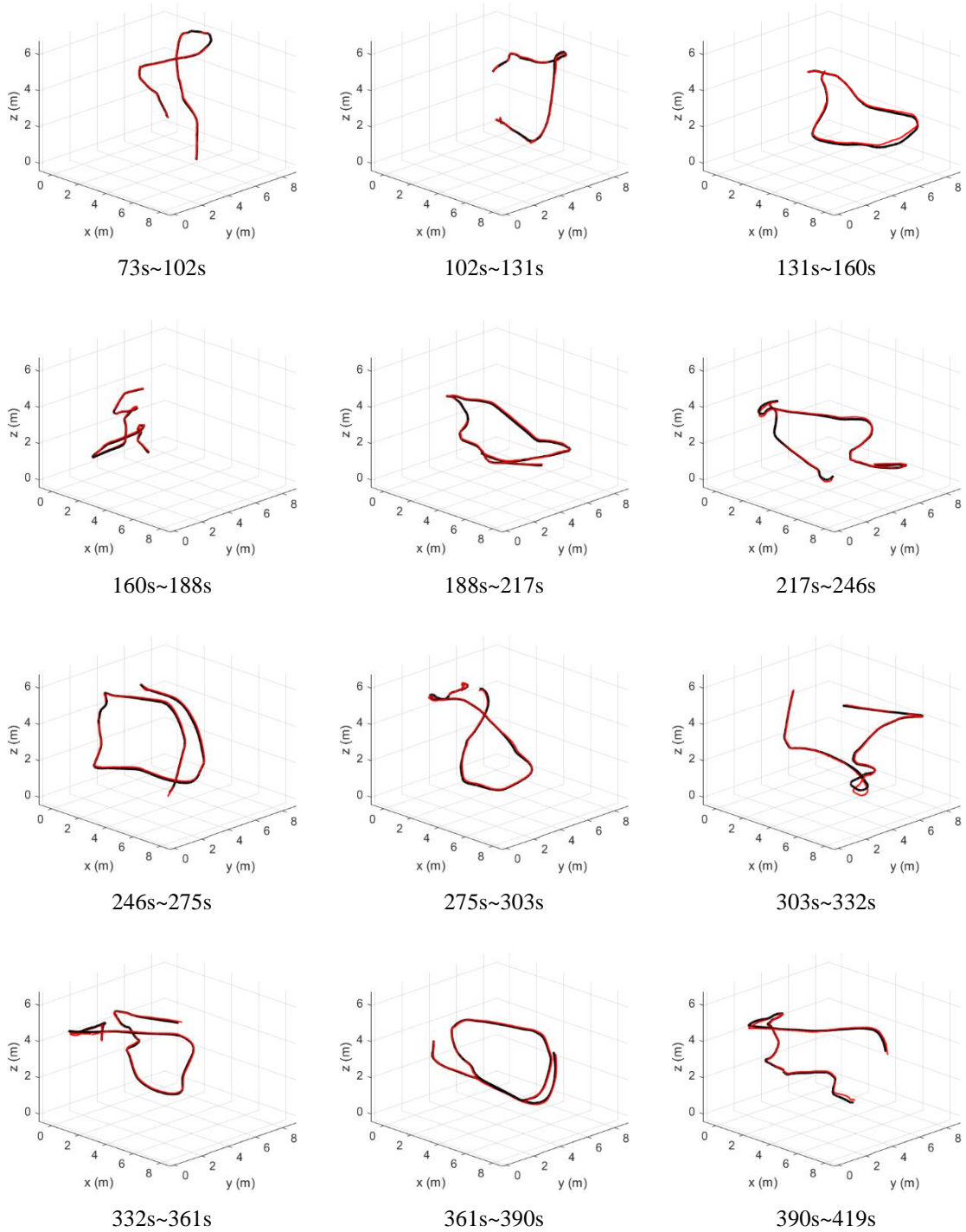


Figure 6.4 Set 3 - ground-truth trajectory(Black) and estimated position(Red) in 3D space.

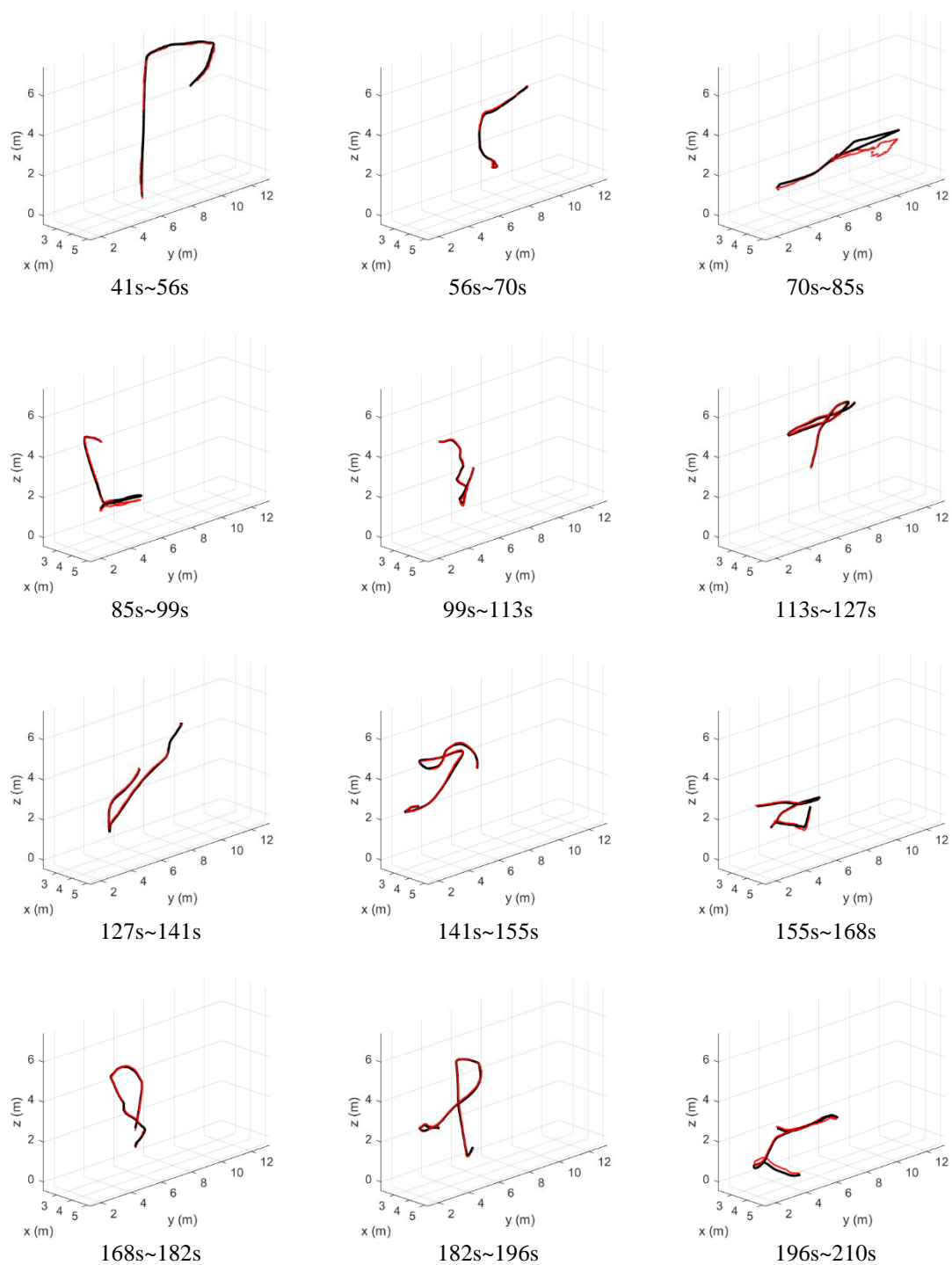


Figure 6.5 Set 4 - ground-truth trajectory(Black) and estimated position(Red) in 3D space.

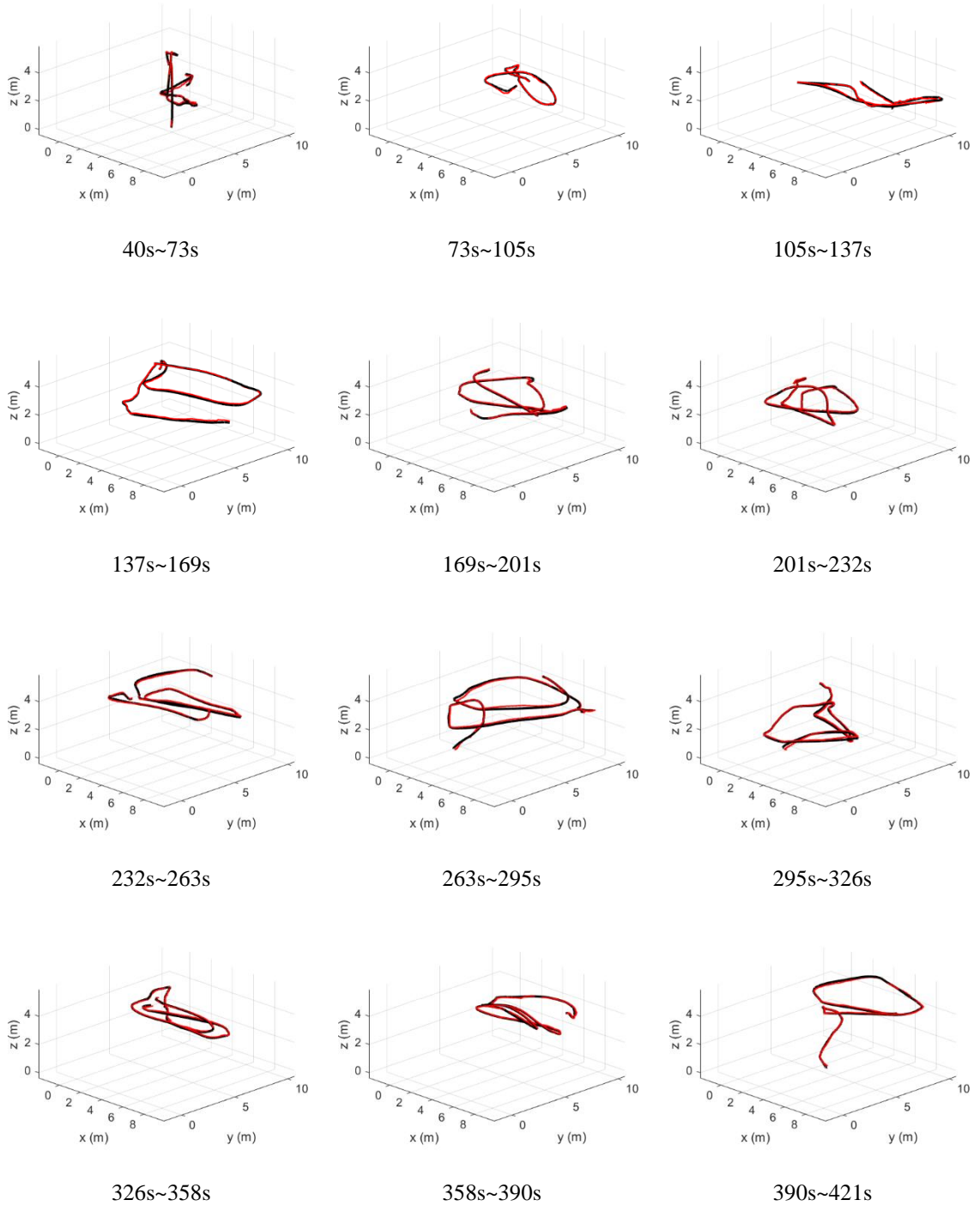
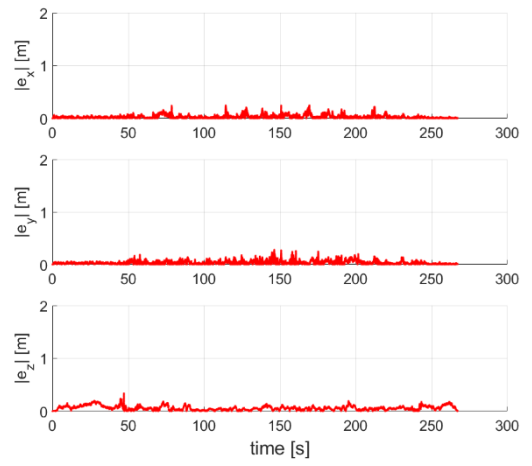
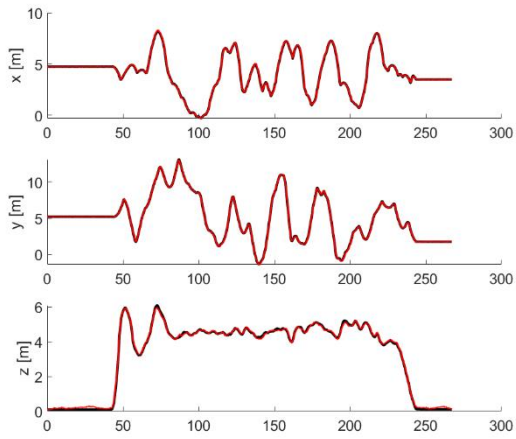
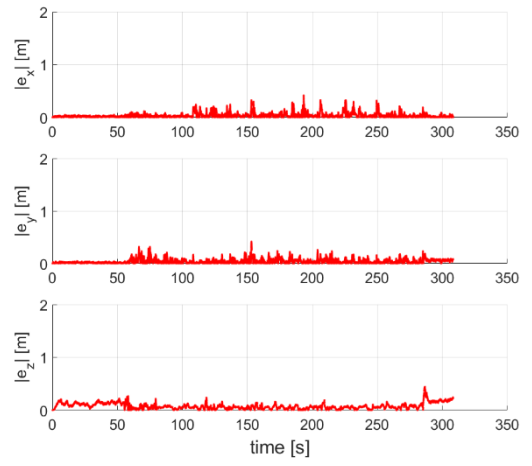
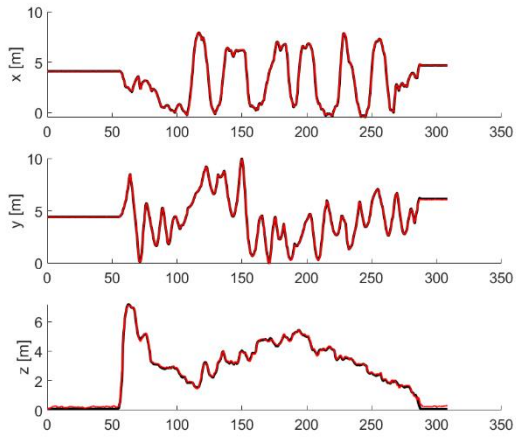


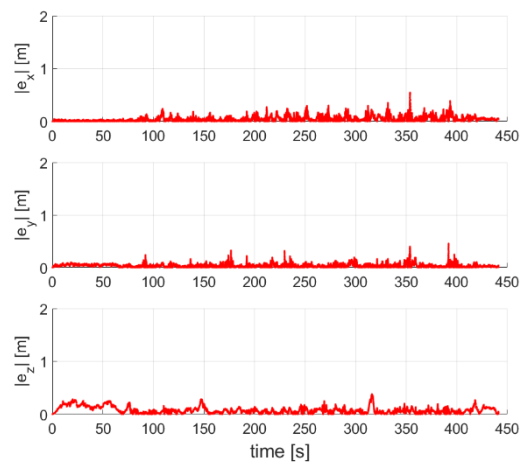
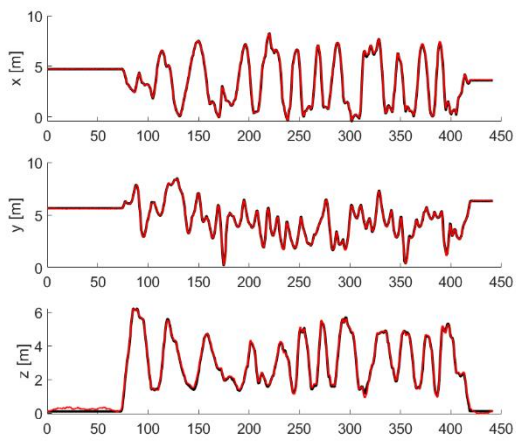
Figure 6.6 Set 5 - ground-truth trajectory(Black) and estimated position(Red) in 3D space.



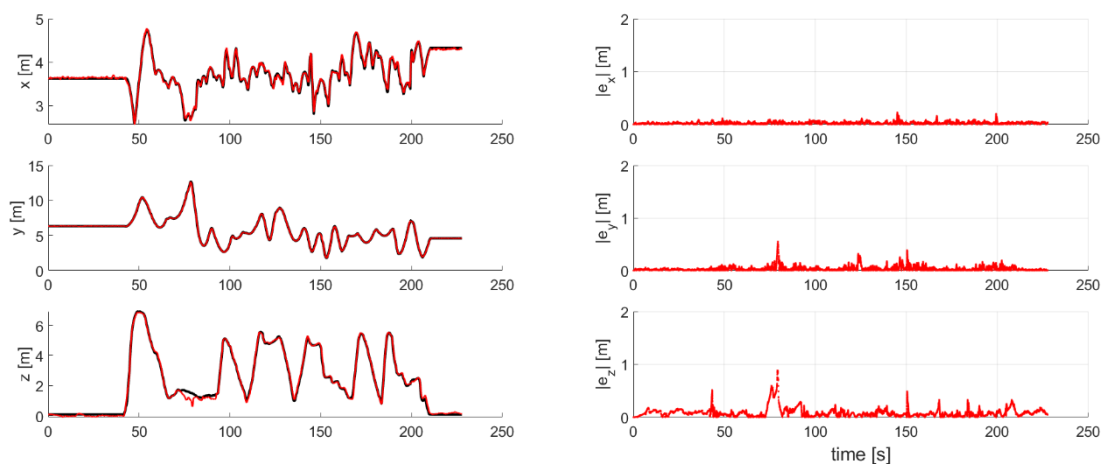
Set 1



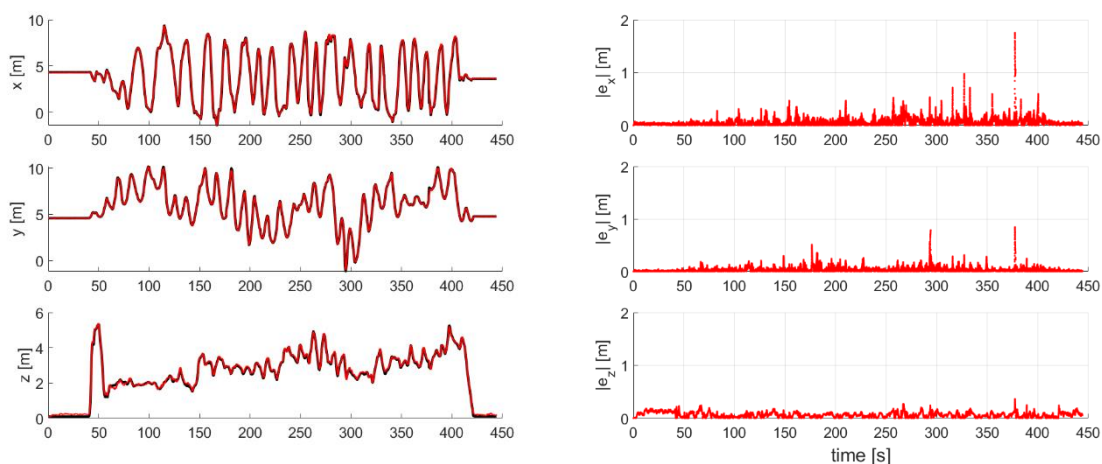
Set 2



Set 3



Set 4



Set 5

Figure 6.7 Ground-truth trajectory and estimated position (left column) and absolute error (right column) over time.

## 6.5 Discussions

### 6.5.1 Influence of height on accuracy

Figure 6.8 (a) shows a graph of absolute errors in the z-direction versus height. The z value of ground truth was divided by 0.1m intervals, and the mean error was calculated. The higher the elevation in all datasets, the smaller the error. I can adopt dilution of precision(DOP) to

explain this situation. The idea of DOP is to know how errors in the measurement affect the final position estimation (Langley & others, 1999). Figure 6.8 (b) shows vertical DOP(VDOP) at the center point (4.12m,5.40m) of our configuration by changing the height from 0m to 8m. VDOP is a minimum value of 90.39 at 4.5m. Due to the current anchor configuration, the VDOP of UAV is very high in all spaces. If I attach a UWB anchor to the ceiling, the VDOP can be much lower. In a real outdoor application, however, the sensor will not be able to be attached to the ceiling so that VDOP will show be a similar tendency.

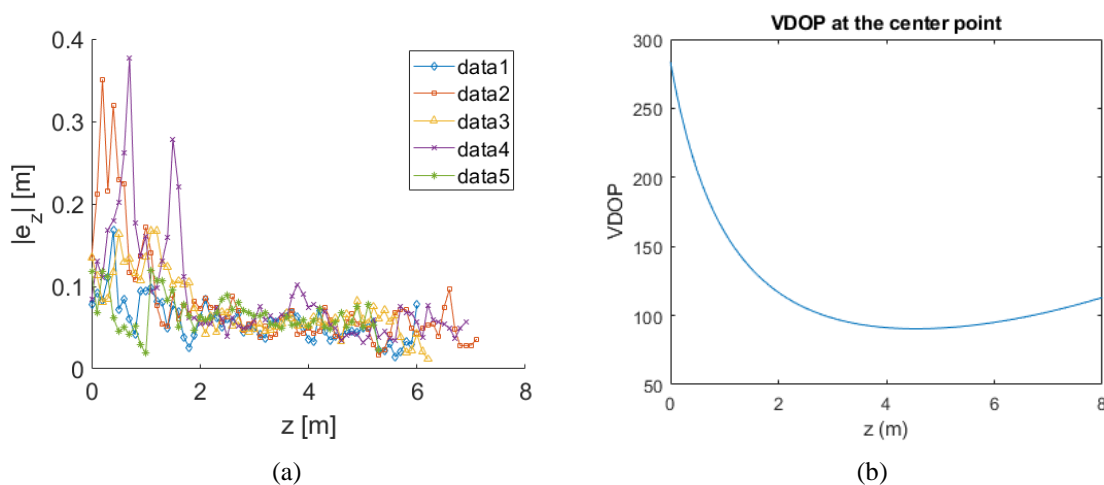


Figure 6.8 (a) Influence of height on z error and (b) VDOP at the center point

### 6.5.2 Influence of velocity on accuracy

Figure 6.9 shows graphs of absolute errors in each direction versus velocity in each axis. In general, as velocity increases, the error also appears to increase linearly. In the x and y directions, this tendency is evident at low speeds. However, at high speeds it can also cause

large errors. In the z directions, I can see the same tendency. However, it also shows various error due to other factors such as VDOP.

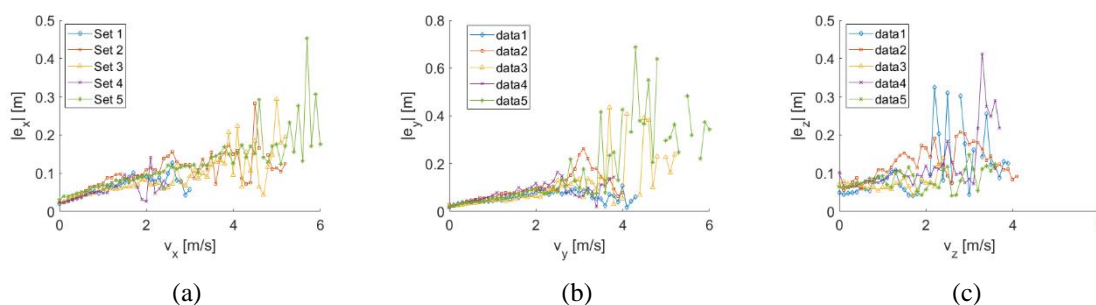


Figure 6.9 Influence of velocity on accuracy: (a) x error vs x velocity, (b) y error vs y velocity and (c) z error vs z velocity.

It is desired to fly UAV less than 2m/s horizontally and 1.5 m/s vertically to have accuracy of 10cm and prevent unexpected huge errors.

## 6.6 Summary

In this chapter, I introduce the EKF based positioning with UWB and IMU fusing. I got result continuously from all time step for EKF. The implementation details of our algorithm was also presented. Average MAE of the five dataset was 0.103m. Low accuracy on height can be improved by fusing with IMU data. Horizontal accuracy was also improved for a few millimetres. Discussions on the accuracy with respect to various condition are presented. VDOP and z-directional accuracy are closely related due to the position of anchors. The larger the VDOP, the higher the error. Also, each axial error and velocity is a linear relationship.

## **Chapter 7**

### **Conclusions and Future works**

#### **7.1 Conclusions**

In this study, I am aimed to develop a UWB based positioning system for GNSS-denied environments. Firstly, many challenges for vertical infrastructure inspection is investigated, which are the major motivations of our study. GNSS-based navigation is the most widely used method, but accuracy does not meet requirements for vertical infrastructure inspections. For this purpose, UWB-based positioning is proposed in this study. I further formulate the main problems into the tasks into the tasks of UWB calibration, benchmark dataset, and two different positioning algorithms multilateration and EKF. Related research work is also reviewed.

UWB calibration was conducted to understand UWB ranging and improve accuracy of positioning by comparing with EDM measurements. As a result, I found linear relation between UWB range true range. This results meet the manufacturers accuracy standard which has less than 2 cm of ranging errors. Average residual, average failure rate, and average standard deviation were investigated. Overall, considering centimeter level accuracy and high frequency, I concluded UWB ranging is suitable for accurate positioning of UAV.

Despite the importance of UWB based UAV positioning, there has been no benchmark dataset provided for the evaluation of the related algorithms. Total of five data set was generated as a benchmark for UAV positioning in GNSS denied environment. Experimental configuration and set up are described.

I developed multilateration method for UWB based UAV positioning. Due to flip ambiguity, I can obtain erroneous estimation by algebraic solution. I developed correction method of flipped solution by inverting the flipped solution with respect to the optimal fitting anchor plane. As a result, the accuracy was greatly improved by correcting the flip-ambiguity. After correction, the solution was refined through nonlinear optimization and improved accuracy.

The limitation of multilateration method is that positioning is possible only when various observations are made in a short time. Also, since most UAVs can use IMU observations, I developed the EKF based positioning with UWB and IMU fusing. A EKF was described and an IMU driven motion model was presented. The positioning is performed by applying EKF to the IMU driven model. As a result, EKF showed better accuracy than multilateration. Discussions on the accuracy with respect to various condition were presented.

## 7.2 Directions for Future Research

Based on the limitation of our research and current development of the field, the future directions of our work are summarized as follows:

- **Applying other Bayesian filtering and smoothing techniques:** There are many additional filtering and smoothing methods to estimate the state of a time-varying system based on various observational inputs. For filtering algorithms, I can also apply iterated Kalman filter (Bell & Cathey, 1993), unscented ("sigma-point") Kalman filter (Julier, 2002), cubature Kalman filter (Arasaratnam & Haykin, 2009),

particle filter (Van Der Merwe, Doucet, De Freitas, & Wan, 2001), H-infinity filter (Burl, 1998), etc. I can also apply smoothing algorithms (Särkkä, 2013).

- **Large scale experiment:** I got our dataset in an indoor environment in chapter 4. To apply our algorithm in the real application, I need to collect datasets in a large scale outdoor environment. In an outdoor large scale environment, it is difficult to obtain ground truth of data set. The GNSS, camera, and Lidar can be integrated to obtain the ground truth and the integrated data set.
- **Efficient installation of UWB anchors and Range-Only Simultaneous Localization and Mapping (RO-SLAM):** For UWB-based positioning, the coordinates of anchors must be known in advance, which requires time-consuming precise surveying, which makes it difficult to apply. RO-SLAM can be applied to solve this problem (Fabresse, Caballero, Maza, & Ollero, 2016). This allows us to perform UWB-based positioning even if there are no pre-installed anchors or less.
- **Positioning with low cost UWBs:** In this study, the positioning of high accuracy UWB modules was performed, but high accuracy UWBs are expensive to cover a wide area. Currently, there are various accuracy UWBs in the market, and it is necessary to study positioning using low-cost UWB to apply to various inspection applications widely.
- **UWB ranging in NLoS situation:** In this study, the positioning was performed in a clear LoS situation. However, the signal often blocked by vertical structures and obstacles. It is essential to classify the NLOS situation and improve UWB ranging to ensure the quality of positioning in cluttered environment.

- **Various sensor integration with current system and inspection:** I can integrate existing systems with other sensors such as Lidar and cameras for vertical infrastructure inspection applications. Integrated system can have higher navigation performance by fusing measurements from various sensors. Various deformation detection method based on inspection metric are required for the actual vertical structure inspection.

## Bibliography

- Abdelkrim, N., Aouf, N., Tsourdos, A., & White, B. (2008). Robust nonlinear filtering for INS/GPS UAV localization. *2008 16th Mediterranean Conference on Control and Automation*, 695–702.
- Alarifi, A., Al-Salman, A., Alsaleh, M., Alnafessah, A., Al-Hadhrami, S., Al-Ammar, M., & Al-Khalifa, H. (2016). Ultra wideband indoor positioning technologies: Analysis and recent advances. *Sensors*, *16*(5), 707.
- Arasaratnam, I., & Haykin, S. (2009). Cubature kalman filters. *IEEE Transactions on Automatic Control*, *54*(6), 1254–1269.
- Balaguer, C., Gimenez, A., & Jardón, A. (2005). Climbing robots' mobility for inspection and maintenance of 3D complex environments. *Autonomous Robots*, *18*(2), 157–169.
- Barral, V., Suárez-Casal, P., Escudero, C. J., & García-Naya, J. A. (2019). Multi-sensor accurate forklift location and tracking simulation in industrial indoor environments. *Electronics*, *8*(10), 1152.
- Bell, B. M., & Cathey, F. W. (1993). The iterated Kalman filter update as a Gauss-Newton method. *IEEE Transactions on Automatic Control*, *38*(2), 294–297.
- Benini, A., Mancini, A., & Longhi, S. (2013). An imu/uwb/vision-based extended kalman filter for mini-uav localization in indoor environment using 802.15.4a wireless sensor network. *Journal of Intelligent & Robotic Systems*, *70*(1–4), 461–476.
- Bhuiyan, M. Z. A., Wang, G., Cao, J., & Wu, J. (2013). Deploying wireless sensor networks with fault-tolerance for structural health monitoring. *IEEE Transactions on Computers*,

64(2), 382–395.

Bishop, G., & Welch, G. (2001). An introduction to the kalman filter. *Proc of SIGGRAPH, Course*, 8(27599–23175), 41.

Bogdani, E., Vouyioukas, D., Nomikos, N., Skoutas, D. N., & Skianis, C. (2015). Angle-based time fingerprint positioning technique for indoor UWB systems. *2015 IEEE International Conference on Communications (ICC)*, 6193–6198.

Bruggemann, T. S., & Ford, J. J. (2013). Automated aerial inspection guidance with improved turn planning. *2013 Australian Control Conference*, 282–288.

Burl, J. B. (1998). *Linear optimal control: H (2) and H (Infinity) methods*. Addison-Wesley Longman Publishing Co., Inc.

Chae, M. J., Yoo, H. S., Kim, J. Y., & Cho, M. Y. (2012). Development of a wireless sensor network system for suspension bridge health monitoring. *Automation in Construction*, 21, 237–252.

Contreras, D., Castro, M., & de la Torre, D. S. (2017). Performance evaluation of bluetooth low energy in indoor positioning systems. *Transactions on Emerging Telecommunications Technologies*, 28(1), e2864.

Eschmann, C., Kuo, C.-M., Kuo, C.-H., & Boller, C. (2013). High-resolution multisensor infrastructure inspection with unmanned aircraft systems. *ISPRS-International Archives of the Photogrammetry, Remote Sensing and Spatial Information Sciences*, (2), 125–129.

Fabresse, F. R., Caballero, F., Maza, I., & Ollero, A. (2016). Robust Range-Only SLAM for Unmanned Aerial Systems. *Journal of Intelligent and Robotic Systems: Theory and*

- Applications*, 84(1–4), 297–310. <https://doi.org/10.1007/s10846-015-0322-z>
- Gaspar, T., & Oliveira, P. (2011). Single pan and tilt camera indoor positioning and tracking system. *European Journal of Control*, 17(4), 414–428.
- Gezici, S., Tian, Z., Giannakis, G. B., Kobayashi, H., Molisch, A. F., Poor, H. V., & Sahinoglu, Z. (2005). Localization via ultra-wideband radios: a look at positioning aspects for future sensor networks. *IEEE Signal Processing Magazine*, 22(4), 70–84.
- Gigl, T., Janssen, G. J. M., Dizdarevic, V., Witrisal, K., & Irahauten, Z. (2007). Analysis of a UWB indoor positioning system based on received signal strength. *2007 4th Workshop on Positioning, Navigation and Communication*, 97–101.
- Golparvar-Fard, M., Bohn, J., Teizer, J., Savarese, S., & Peña-Mora, F. (2011). Evaluation of image-based modeling and laser scanning accuracy for emerging automated performance monitoring techniques. *Automation in Construction*, 20(8), 1143–1155.
- Guo, K., Qiu, Z., Miao, C., Zaini, A. H., Chen, C. L., Meng, W., & Xie, L. (2016). Ultra-wideband-based localization for quadcopter navigation. *Unmanned Systems*, 4(01), 23–34.
- Haynes, G. C., Khripin, A., Lynch, G., Amory, J., Saunders, A., Rizzi, A. A., & Koditschek, D. E. (2009). Rapid pole climbing with a quadrupedal robot. *2009 IEEE International Conference on Robotics and Automation*, 2767–2772.
- Julier, S. J. (2002). The scaled unscented transformation. *Proceedings of the 2002 American Control Conference (IEEE Cat. No. CH37301)*, 6, 4555–4559.
- Kanellakis, C., Fresk, E., Mansouri, S. S., Kominiak, D., & Nikolakopoulos, G. (2019). Autonomous visual inspection of large-scale infrastructures using aerial robots. *ArXiv*

*Preprint ArXiv:1901.05510.*

- Kim, S., Spenko, M., Trujillo, S., Heyneman, B., Santos, D., & Cutkosky, M. R. (2008). Smooth vertical surface climbing with directional adhesion. *IEEE Transactions on Robotics*, 24(1), 65–74.
- Ksentini, D., Elhadi, A. R., & Lasla, N. (2014). Inertial measurement unit: evaluation for indoor positioning. *2014 International Conference on Advanced Networking Distributed Systems and Applications*, 25–30.
- Langley, R. B., & others. (1999). Dilution of precision. *GPS World*, 10(5), 52–59.
- Li, H. (2014). Low-cost 3d bluetooth indoor positioning with least square. *Wireless Personal Communications*, 78(2), 1331–1344.
- Li, K., Wang, C., Huang, S., Liang, G., Wu, X., & Liao, Y. (2016). Self-positioning for UAV indoor navigation based on 3D laser scanner, UWB and INS. *2016 IEEE International Conference on Information and Automation (ICIA)*, 498–503.
- Liu, H., Darabi, H., Banerjee, P., & Liu, J. (2007). Survey of wireless indoor positioning techniques and systems. *IEEE Transactions on Systems, Man, and Cybernetics, Part C (Applications and Reviews)*, 37(6), 1067–1080.
- Liu, W., Dong, E., & Song, Y. (2016). Analysis of flip ambiguity for robust three-dimensional node localization in wireless sensor networks. *Journal of Parallel and Distributed Computing*, 97, 57–68.
- Long, C., Shen, C., Feng, G., Zhu, Y., & Wang, Z. (2016). Research on network scalability based on uwb indoor localization system. *MATEC Web of Conferences*, 42, 7003.
- Luna, M., Meifeng, G., Xinxu, Z., Yongjian, Z., & Mingliang, S. (2015). An indoor

- pedestrian positioning system based on inertial measurement unit and wireless local area network. *2015 34th Chinese Control Conference (CCC)*, 5419–5424.
- Mao, C., Lin, K., Yu, T., & Shen, Y. (2018). A Probabilistic Learning Approach to UWB Ranging Error Mitigation. *2018 IEEE Global Communications Conference (GLOBECOM)*, 1–6.
- Mautz, R., Ochieng, W., Brodin, G., & Kemp, A. H. (2007). 3D Wireless Network Localization from Inconsistent Distance Observations. *Ad Hoc & Sensor Wireless Networks*, 3(2–3), 141–170.
- McLoughlin, B., Cullen, J., Shaw, A., & Bezombes, F. (2018). Towards an Unmanned 3D Mapping System Using UWB Positioning. *Annual Conference Towards Autonomous Robotic Systems*, 416–422.
- Miraglia, G., Maleki, K. N., & Hook, L. R. (2017). Comparison of two sensor data fusion methods in a tightly coupled UWB/IMU 3-D localization system. *2017 International Conference on Engineering, Technology and Innovation (ICE/ITMC)*, 611–618.
- Neburka, J., Tlamsa, Z., Benes, V., Polak, L., Kaller, O., Bolecek, L., ... Kratochvil, T. (2016). Study of the performance of RSSI based Bluetooth Smart indoor positioning. *2016 26th International Conference Radioelektronika (RADIOELEKTRONIKA)*, 121–125.
- Nekoogar, F. (2005). Introduction to ultra-wideband communications. *UltraWideband Communications Fundamentals and Applications*, 1–44.
- Nemra, A., & Aouf, N. (2010). Robust INS/GPS sensor fusion for UAV localization using SDRE nonlinear filtering. *IEEE Sensors Journal*, 10(4), 789–798.

- Norrdine, A. (2012, November). An algebraic solution to the multilateration problem. In *Proceedings of the 15th international conference on indoor positioning and indoor navigation, Sydney, Australia* (Vol. 1315).
- Perez-Grau, F. J., Caballero, F., Merino, L., & Viguria, A. (2017). Multi-modal mapping and localization of unmanned aerial robots based on ultra-wideband and RGB-D sensing. *2017 IEEE/RSJ International Conference on Intelligent Robots and Systems (IROS)*, 3495–3502.
- Perttula, A., Leppäkoski, H., Kirkko-Jaakkola, M., Davidson, P., Collin, J., & Takala, J. (2014). Distributed indoor positioning system with inertial measurements and map matching. *IEEE Transactions on Instrumentation and Measurement*, 63(11), 2682–2695.
- Qigao, F., Biwen, S., & Yaheng, W. (2015). Tightly coupled model for indoor positioning based on uwb/ins. *International Journal of Computer Science Issues (IJCSI)*, 12(4), 11.
- Rady, S., Kandil, A. A., & Badreddin, E. (2011). A hybrid localization approach for uav in gps denied areas. *2011 IEEE/SICE International Symposium on System Integration (SII)*, 1269–1274.
- Raza, U., Khan, A., Kou, R., Farnham, T., Premalal, T., Stanoev, A., & Thompson, W. (2019). Dataset: Indoor Localization with Narrow-band, Ultra-Wideband, and Motion Capture Systems. *Proceedings of the 2nd Workshop on Data Acquisition To Analysis*, 34–36.
- Ruan, T., & Balch, R. (2018). RPM measurement using MEMS Inertial Measurement Unit (IMU). *Proceedings of the International Conference on Embedded Systems, Cyber-*

*Physical Systems, and Applications (ESCS)*, 49–53.

Ruiz, A. R. J., & Granja, F. S. (2017). Comparing ubisense, bespoon, and decawave uwb location systems: Indoor performance analysis. *IEEE Transactions on Instrumentation and Measurement*, 66(8), 2106–2117.

Sa, I., & Corke, P. (2014a). Close-quarters Quadrotor flying for a pole inspection with position based visual servoing and high-speed vision. *2014 International Conference on Unmanned Aircraft Systems (ICUAS)*, 623–631.

Sa, I., & Corke, P. (2014b). Vertical infrastructure inspection using a quadcopter and shared autonomy control. *Field and Service Robotics*, 219–232.

Särkkä, S. (2013). *Bayesian filtering and smoothing* (Vol. 3). Cambridge University Press.

Shahbazi, M., Sohn, G., Théau, J., & Menard, P. (2015). Development and evaluation of a UAV-photogrammetry system for precise 3D environmental modeling. *Sensors*, 15(11), 27493–27524.

Shi, G., & Ming, Y. (2016). Survey of indoor positioning systems based on ultra-wideband (UWB) technology. In *Wireless Communications, Networking and Applications* (pp. 1269–1278). Springer.

Sohn, S., Lee, B., Kim, J., & Kee, C. (2008). Vision-based real-time target localization for single-antenna GPS-guided UAV. *IEEE Transactions on Aerospace and Electronic Systems*, 44(4), 1391–1401.

Tiemann, J., Eckermann, F., & Wietfeld, C. (2016a). Atlas-an open-source tdoa-based ultra-wideband localization system. *2016 International Conference on Indoor Positioning and Indoor Navigation (IPIN)*, 1–6.

- Tiemann, J., Eckermann, F., & Wietfeld, C. (2016b). Multi-user interference and wireless clock synchronization in TDOA-based UWB localization. *2016 International Conference on Indoor Positioning and Indoor Navigation (IPIN)*, 1–6.
- Tiemann, J., Ramsey, A., & Wietfeld, C. (2018). Enhanced UAV indoor navigation through SLAM-augmented UWB localization. *2018 IEEE International Conference on Communications Workshops (ICC Workshops)*, 1–6.
- Tisdale, J., Ryan, A., Kim, Z., Tornqvist, D., & Hedrick, J. K. (2008). A multiple UAV system for vision-based search and localization. *2008 American Control Conference*, 1985–1990.
- Van Der Merwe, R., Doucet, A., De Freitas, N., & Wan, E. A. (2001). The unscented particle filter. *Advances in Neural Information Processing Systems*, 584–590.
- Vinayak, K. V. (2010). *A study on high-speed low-power ultra-wideband transceiver for short-range wireless communications*.
- Viswanathan, S., & Srinivasan, S. (2015). Improved path loss prediction model for short range indoor positioning using bluetooth low energy. *2015 IEEE SENSORS*, 1–4.
- Wang, C., Zhang, H., Nguyen, T.-M., & Xie, L. (2017). *Ultra-Wideband Aided Fast Localization and Mapping System*. Retrieved from <http://arxiv.org/abs/1710.00156>
- Wang, Y., Leus, G., & Deliç, H. (2009). TOA estimation using UWB with low sampling rate and clock drift calibration. *2009 IEEE International Conference on Ultra-Wideband*, 612–617.
- Welch, G., & Bishop, G. (1995). *An introduction to the Kalman filter*.
- Zahran, S., Mostafa, M. M., Masiero, A., Moussa, A. M., Vettore, A., & El-Sheimy, N.

(2018). MICRO-RADAR AND UWB AIDED UAV NAVIGATION IN GNSS DENIED ENVIRONMENT. *International Archives of the Photogrammetry, Remote Sensing & Spatial Information Sciences*, 42(1).